Accepted Manuscript

Lower Pliensbachian caldera volcanism in high-obliquity rift systems in the western North Patagonian Massif, Argentina

Leonardo Benedini, Daniel Gregori, Leonardo Strazzere, Juan I. Falco, Jorge A. Dristas

PII: S0895-9811(14)00093-5

DOI: 10.1016/j.jsames.2014.08.001

Reference: SAMES 1296

To appear in: *Journal of South American Earth Sciences*

Received Date: 17 June 2014

Revised Date: 26 July 2014

Accepted Date: 5 August 2014

Please cite this article as: Benedini, L., Gregori, D., Strazzere, L., Falco, J.I., Dristas, J.A., Lower Pliensbachian caldera volcanism in high-obliquity rift systems in the western North Patagonian Massif, Argentina, *Journal of South American Earth Sciences* (2014), doi: 10.1016/j.jsames.2014.08.001.

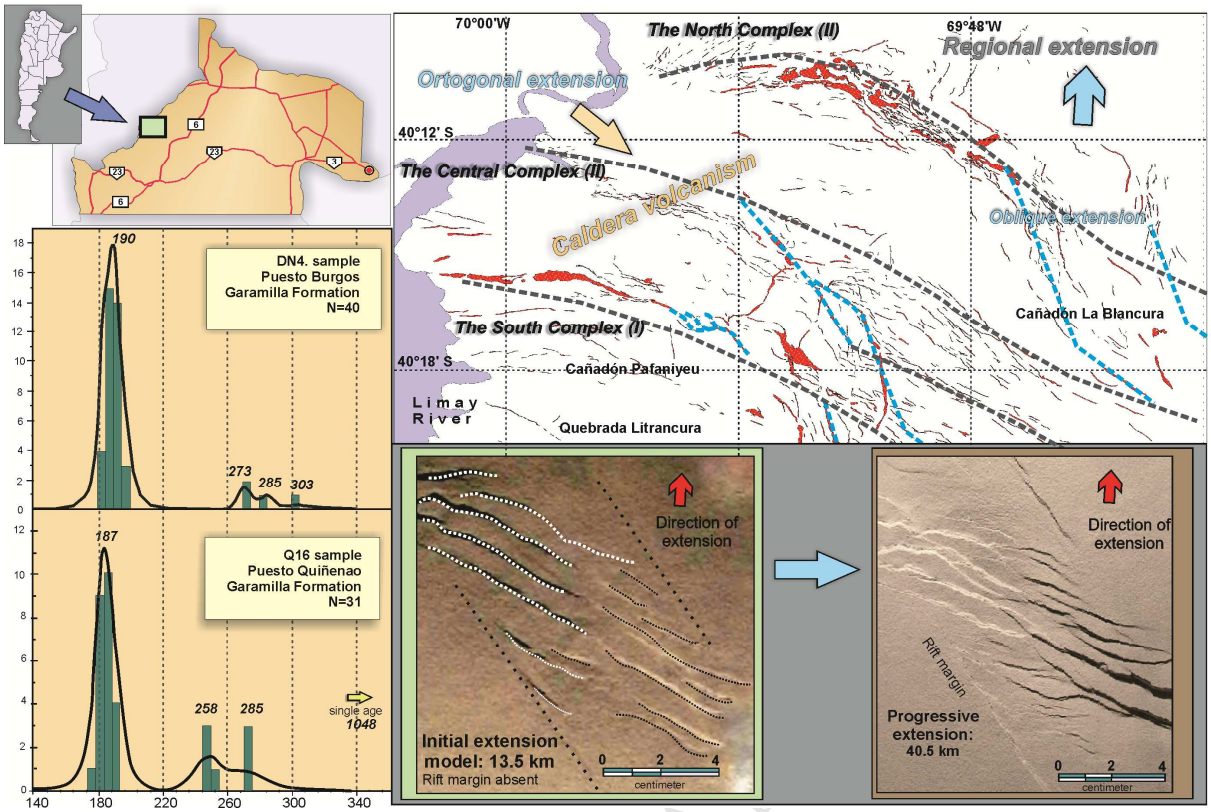

Lower Pliensbachian caldera volcanism in high-obliquity rift systems in the western North Patagonian Massif, Argentina

Leonardo Benedini[1]*, Daniel Gregori[1], Leonardo Strazzere[1], Juan I. Falco[1], Jorge A. Dristas[2]

[1] INGEOSUR, Cátedra de Geología Argentina, Departamento de Geología, Universidad Nacional del Sur, San Juan 670, 8000 Bahía Blanca, Argentina

[2] INGEOSUR, Cátedra de Petrología, Departamento de Geología, Universidad Nacional del Sur, San Juan 670, 8000 Bahía Blanca, Argentina

* Corresponding author. Tel.: 54 291 4595101x3031. E-mail addresses: lbenedini@criba.edu.ar (L. Benedini), usgregor@criba.edu.ar (D. Gregori), leostrazzere@hotmail.com (L. Strazzere), falco.juan@gmail.com.ar (J. Falco), jdristas@uns.edu.ar (J. Dristas)

ABSTRACT:

In the Cerro Carro Quebrado and Cerro Catri Cura area, located at the border between the Neuquén Basin and the North Patagonian Massif, the Garamilla Formation is composed of four volcanic stages: 1) andesitic lava-flows related to the beginning of the volcanic system; 2) basal massive lithic breccias that represent the caldera collapse; 3) voluminous, coarse-crystal rich massive lava-like ignimbrites related to multiple, steady eruptions that represent the principal infill of the system; and, finally 4) domes, dykes, lava flows, and lava domes of rhyolitic composition indicative of a post-collapse stage.

The analysis of the regional and local structures, as well as, the architectures of the volcanic facies, indicates the existence of a highly oblique rift, with its principal extensional strain in a NNE–SSW direction (~N10°).

The analyzed rocks are mainly high-potassium dacites and rhyolites with trace and RE elements contents of an intraplate signature. The age of these rocks (189± 0.76 Ma) agree well with other volcanic sequences of the western North Patagonian Massif, as well as, the Neuquén Basin, indicating that Pliensbachian magmatism was widespread in both regions. The age is also coincident with phase 1 of volcanism of the eastern North Patagonia Massif (188–178 Ma) represented by ignimbrites, domes, and pyroclastic rocks of the Marifil Complex, related to intraplate magmatism.

Key words: Garamilla Formation, Pliensbachian magmatism, North Patagonian Massif, Argentina.

1. Introduction and regional settings

The North Patagonian Massif (Northern Patagonia, Argentina) is a crustal block of 140,000 km^2 with a complex igneous history. It is characterized by extensive Lower to Middle Jurassic bimodal volcanic deposits that overlay unconformably Upper Paleozoic granites and are covered by Tertiary sediment and basaltic rocks.

The Lower Jurassic volcanic deposits in northern Patagonia can be separated into two principal domains: the western domain, located mainly in the Patagonian Andes, and the extra-Andean domain, mostly represented by the North Patagonian Massif of central Patagonia and the Atlantic coast (Fig. 1). Both, the western and eastern domains involve important volcanic and sedimentary successions. The Andean domain is mainly represented by the Subcordilleran Batholith (Gordon and Ort, 1993) or the Subcordilleran Belt (SCB; Haller et al., 1999; Rapela et al., 2005). It consists of a discontinuous belt of Early Jurassic igneous rocks and sediments that extend for more than 250 km and which represent an oblique batholith developed during the Upper Triassic–Lower Jurassic time. The Liassic sediments interbedding in the volcanic rocks have been assigned to an intra-arc setting (Page and Page, 1999) or to a Toarcian retro-arc basin (Suárez and Marquez, 2007).

The extra-Andean domain involves the North Patagonian Massif. The Lower Jurassic deposits recorded there consist of intermediate to acidic volcanic rocks that are grouped into five major volcanic units: the Marifil Complex (Malvicini and Llambías, 1974), Taquetrén Formation (Nullo and Proserpio, 1975), Sañicó Formation (Stipanicic et al., 1968), Garamilla Formation (Nullo, 1978), and Lonco Trapial Formation (Lesta and Ferello,

1972), whose relationships and genetic significance, and even ages, are partly unknown.

The Marifil Complex crops out in the eastern area of the massif, from the Sierra de Pailemán (NE Río Negro Province) to the Chubut River (central Chubut Province), along 400 km N–S. It is composed of a thick sequence of volcanic breccias, tuffs, ignimbrites, and subvolcanic acidic bodies of a Lower Pliensbachian age (K/Ar age of 189 ± 5 Ma) obtained south of the Sierra Grande (Cortés, 1981).This age has later been roughly confirmed by several authors (Rapela and Pankhurst, 1993;Alric et al., 1996;Féraud et al. 1999). Pankhurst and Rapela (1995) proposed a genetic evolution of this unit due to the anatexis of the Patagonian Mesoproterozoic lower crust, and considered that the dacite-rhyolite suite of this unit was formed by crystal-liquid fractionation processes derived from primary andesites. Later, Pankhurst et al. (2000) included this unit within the first volcanic event (V1) related to the major episode of pre-Gondwana breakup.

The western sector of the North Patagonian Massif is represented by two volcanic units whose genetic evolution is not completely understood.

The Taquetrén and Garamilla formations are widespread, and are represented between the Limay River (Neuquén Province) and the Sierra de Taquetrén (Chubut Province) by compositional and lithological differences. The Taquetrén Formation consists of breccias, lavas, and a lesser amount of tuffs and ignimbrites of andesitic composition. This unit is related to epiclastic sediments that were initially assigned to the Late Jurassic by Nullo and Proserpio (1975) on the basis of flora fossil remains. Later, the unit was

assigned to the Liassic by Escapa et al. (2008) on the basis of the presence of taxas such as *Goeppertertella*, *Sagenopteris*, *Clathropteris*, and *Archangelskya*.

The Taquetrén Formation was considered by Lizuaín and Silva Nieto (2005) to be volcaniclastic facies of the Lonco Trapial Formation, included in the Cañadón Asfalto Basin, and therefore sharing a common origin. This basin was considered to be a pull-apart (Silva Nieto et al.,2002) that developed in the southern part of the North Patagonian Massif, whose sedimentation started in the Middle Jurassic and ended at the Tithonian time. (All ages accord with the International stratigraphic chart, International Commission on Stratigraphy, 2009).

Recently, Cúneo et al. (2013) have obtained U/Pb zircon ages for the Lonco Trapial Formation of 188 and 178 Ma (Pliensbachian–Toarcian),being therefore the Lonco Trapial and Taquetrén Formation coeval with the V1 Marifil Complex event and the Garamilla Formation (188 and 187 Ma) (Franzese et al., 2002;Benedini and Gregori, 2013).

As indicated above, the Garamilla Formation outcrop is in the western sector of the North Patagonian Massif, near the Limay River. There, in the Puesto Fuensalida-Quiñenao area, the unit was extensively analyzed by Benedini and Gregori (2013), who recognized three volcanic sequences. The first one comprises lava-like ignimbrites, porphyritic massive rhyolites, and microgranular massive rhyolites. The second is composed of porphyritic massive andesites and dacites, lapilli-tuffs and eutaxitic lapilli-tuffs of dacitic composition. The third unit includes tuffs, lapilli-tuffs, massive tuff-breccias, massive lithic breccias, and porphyritic massive and flow-banded rhyolites. The unit reveals a progressive change from normal a calc-alkaline trend in an initial

subduction-related setting to a high-K calc-alkaline series of an intraplate-related setting. These volcanic episodes are temporally and geochemically equivalent to those volcanic units located in half-grabens in several areas of the Neuquén Basin Benedini and Gregori (2013).

The Puesto Fuensalida-Quiñenao area has been interpreted as a transtensional half-graben, whereas others exhibit a trapdoor structure (Benedini and Gregori, 2013). The lineament trends that bound the volcanic system have also been recognized in the western North Patagonian Massif.

New, exhaustive field observation along the Limay River allow us to recognize, in the Cerro Carro Quebrado-Cerro Catri Cura area, a new depocenter of the Garamilla Formation (more than 50 km^2), which was previously unknown (Fig. 2).

The aim of this paper is to establish the configuration and evolution of the Garamilla Formation in this new area located in the western margin of the North Patagonian Massif, based on mapping, profiling, petrography, and geochemical studies. We wish to determine the structural emplacement of the volcanic system and its relationship with the Fuensalida-Quiñenao depocenter.

This information, together with geochemical data and correlation with other areas in the Río Negro Province, leads to the postulation of a preliminary tectonic model for this unit during Lower Jurassic times.

2. Field and laboratory methods

Stratigraphic profiling and facies analysis were the initial methods used to characterize the deposits of the Garamilla Formation. Two detailed profiles were

made in the Cerro Carro Quebrado and Cerro Catri Cura areas, as shown in Fig. 2. Two extra profiles were made outside the studied area, near to Cerro Bayo, (Fig. 10) in order to analyze the configuration of the dyke system located in these areas.

To acquire a preliminary draft of the structural lineaments, faults, body boundaries of the area, gravity and magnetometric data were obtained during a regional geophysical survey of the western sector of the North Patagonian Massif. The gravity and magnetometric data, which are not included in this paper, were combined with mapping and profiling to produce compound profiles to model the studied area.

Field work together with detailed petrography and preliminary geochemistry studies were made of selected samples to interpret eruption conditions, as well as chemical evolution during the deposition of the Garamilla Formation. More than 155 samples were collected during the field work. Detailed petrography was undertaken to (i) characterize the components and texture of the ignimbrite facies and (ii) define the stratigraphic characteristics of these volcanic units.

From these samples, 37 thin sections were studied to determine the abundance of the main components of the ignimbrites and, importantly, to help define vertical and lateral variations. The population of free crystals in the matrix was therefore used to distinguish different facies compositions and sub-facies, using image analysis to obtain semi-quantitative data on the crystal size distributions.

Preliminary geochemistry and geochronology was performed in an ACTLAB laboratory and at the Arizona LaserChron Center, Department of

Geosciences, Arizona University, in order to obtain information about volcanic evolution and the time of emplacement in the volcanic system. X-ray fluorescence was used for major and trace elements, whereas the rare earth (RE) elements were determined by inductively coupled plasma mass spectrometry.

International geostandards were used to check the precision and accuracy of the results. The procedures described by Gehrels et al. (2008) were used for the geochronological analyses.

3. Results

3.1. Local geology: Garamilla Formation facies analysis

The Garamilla Formation has a generally massive, coherent and uniform character. For lithofacies of pyroclastic origin our study approach largely followed Branney and Kokelaar (2002) while for effusive facies it followed Mc Phee et al. (1993). The lithofacies associations were therefore interpreted using the descriptive facies model of Branney and Kokelaar (2002). The facies subdivision was difficult and was based mainly on the size, sorting, and estimated crystal and lithic clast content and unconformities. The lithofacies association was identified as a portion of the inner cauldron deposit complex that appeared to be comparable with those described earlier by Benedini and Gregori (2013).

The information attained during the mapping and profiling shows regional variations, resulting in the identification of eight distinctive lithofacies: Lithofacies I: flow-banded andesites, Lithofacies II: massive lithic breccias, Lithofacies III: massive lithic-rich eutaxitic lapilli-tuffs, Lithofacies IV: lava-like ignimbrites, Lithofacies V: massive crystal-rich eutaxitic lapilli-tuffs, Lithofacies

VI, VII, and VIII: flow banded rhyolites, massive rhyolites, and jigsaw breccias, respectively (Fig. 2).

3.1.1 Lithofacies I: flow-banded andesites

This lithofacies presents a restricted distribution in the study area, being recognized near the Cerro Carro Quebrado and Cerro Catri Cura. The rocks are dark blue and (Fig. 3A) are horizontally covered by Lithofacies II and intruded by rhyolitic dykes near Cerro Carro Quebrado. These rocks lie unconformably over a pale-grey Lower Permian granite.

This facies shows a 2 cm to 10 cm thick flow banding, developing a porphyritic texture composed by subhedral crystals of plagioclase of 4 mm in diameter, and lesser amphibole phenocrysts embedded in a pilotaxitic groundmass (Fig 3B).

The mineralogy includes plagioclase, amphibole, biotite, quartz, and accessory minerals such as magnetite and apatite in a devitrified groundmass. Phenocryst sizes range from 0.5 to 10 mm.

3.1.2 Lithofacies II: massive lithic breccias

These breccias appear in the southern sector, between Cerro Carro Quebrado and Cerro Curi Mahuida, covering the small outcrops of the andesitic facies.

The massive lithic breccias are a coarse, blue to violet rock. The sub-rounded to sub-angular clasts vary between ash, coarse-lapilli, and blocks. It comprises clasts from older units, including granites and flow-banded andesites. Lithic-rich facies form approximately 50% of the deposit. Its lower part is

dominated by granitic clasts. In the middle part of the sequence lithic fragments appear to be of a dacitic and andesitic composition, which are predominant at the top of the volcanic pile.

The deposit is poorly sorted, showing a normal grading, passing transitionally from a welded base to a matrix supported breccias and lapilli-tuff at the top. As observed in Fig. 3 C, the block composition is dominated by an accidental clast of granites immersed in thin lapilli with ash matrix. The interstitial groundmass includes K-feldspar free crystals (0.5–4 mm long).

3.1.3 Lithofacies III: massive lithic-rich eutaxitic lapilli-tuffs

The massive lithic-rich eutaxitic lapilli-tuff of dacitic composition appears to form a continuous outcrop that covers 5.5 km^2 and presents an estimated thickness of 130 m. In the southern area it is overlaying the massive lithic breccias facies. Fiammes are not easily recognized in the field in the lithic-rich levels. These volcanic deposits are not well preserved and are characterized by a blue to pale pink eutaxitic lapilli-tuff (emLT). They show a vertical gradational change from massive at the base to a diffuse and pseudo-parallel fining towards the top.

As in the lithofacies described above, granite blocks are the most abundant accidental clasts, together with clasts of dacitic lavas. The block compositions change gradually, incorporating progressively more co-magmatic volcanic fragments from previous eruptions into the upper section of the deposits. In thin sections this facies exhibits abundant ash-size lithic fragments (Fig. 3D), followed by subhedral to anhedral K-feldspar crystals fragments, plagioclase, quartz, and hornblende embedded in a vitrophyric groundmass.

Eutaxitic textures are represented by partially sericitic fiammes. The K-feldspar crystalloclasts show reaction borders due to thermal contraction. Fine-grained mica and chlorite are present as alteration products. Accessory minerals include zircon and apatite. The top of these deposits shows marked thin bedding, as shown in Fig. 3E.They are partially devitrified and the crystal components and lithic clasts are oriented to mostly follow the bedding. This feature could be interpreted in terms of a primary depositional characteristic or as the product of diagenetic compaction (syntectonic stage; Allen and Cas, 1990; Branney and Sparks, 1990).

3.1.4 Lithofacies IV: lava-like ignimbrites

The rhyolitic lava-like ignimbrites are pale-orange and consist of thick compound pyroclastic units that have a total thickness estimated at 420 m. This lithofacies covers in erosional unconformity the previous volcanic deposits (Fig. 3E). These rocks crop out 500 m northward of the Cerro Quemado and they occupy more than 12 $km^2$of the central portion of the studied area.

Thin and locally basal fine-grained deposits were recognized underlying the thick massive facies (Fig. 4A). The ignimbritic deposits are intensely welded, and juvenile fragments were modified by loading and the intrusion of acidic dykes and extrusion of lava domes. Flattened pumice fragments are often difficult to recognize in the hand samples.

These rocks present a crystal-rich matrix (30 vol.%) and low lithic contents (1–2vol.%),together with quartz, K-feldspar, plagioclasa, biotite, and hornblende. Accessory minerals are apatite, Fe-oxides, and zircon, while

secondary minerals are calcite, chlorite, sericite, and epidote, which appear randomly distributed in a tuff groundmass.

The matrix exhibits the neoformation of euhedral quartz crystals and triple point contact in some of the specimens, indicative of static recrystallization (Fig. 4B).A few sub-rounded clasts of granite and coherent clasts of andesitic composition were recognized.

3.1.5 Lithofacies V: massive crystal-rich eutaxitic lapilli-tuffs

This lithofacies appears mainly as a discontinuous patch over the margins of the central outcrop of Lithofacies IV. The major outcrop is located south of the Cerro Pafaniyeu, where it covers Lithofacies I and II and is intruded by a complex rhyolitic dyke swarm.

This lithofacies can be separated from the previous one because of the different small lithic fragment concentrations, the amount of free crystal in the matrix, their spatial distribution, the presence of fiammes and the completely different spectral signature in the satellite imagery.

The colour of this lithofacies is pale-brown and shows a diffuse to massive texture (Fig. 4C) characterized by a fine crystal-rich groundmass with a variable juvenile clast population and with well-preserved eutaxitic textures (Fig. 4D).

The deposits are intensely welded with flattened “flame like” fiammes, easily recognized in hand samples. They present quartz, K-feldspar, plagioclase, biotite, and hornblende. The accessory minerals are apatite, Fe oxides, zircon, and the secondary minerals are calcite, chlorite, sericite, and epidote. Where present, the thickness of the deposit ranges from 150 to 25 m. The basal contact is sharp and unconformable with Lithofacies III. The upper

contacts are limited by lavas and lava domes, whereas it is intruded by a fluidal rhyolitic dyke swarm.250 m northwest of the Cerro Pafaniyeu.

3.1.6 Lithofacies VI, VII and VIII: flow-banded rhyolites, massive rhyolites and jigsaw breccias

These three lithofacies are the principal components in lava, lava domes, and dykes or eruptive fractures, which were recognized on the basis of the morphology criteria proposed by Cas and Wright (1987), among others. Fluidal rhyolitic dykes intrude the previous pyroclastic sequences. The flow banded rhyolites and the massive rhyolites show isolated and discontinuous outcrops and are disposed mainly at the margins of the central outcrop, showing a half-moon like distribution (Fig. 5) and displaying subcircular bodies of 700–200 m in diameter.

The flow banded rhyolite facies (Fig. 6A) are characterized by fine-grained 250 μm spherulitic aggregates immersed in a felsitic groundmass (Fig. 6B). Its mineral associations consist of quartz and K-feldspar, with accessory apatite, Fe oxides, biotite, and amphibole. A common feature of these rocks is the presence of spherulite-rich and poor bands, as indicated in Fig. 6A.

The massive rhyolite facies show a rounded shape with cooling joints randomly distributed along their vertical exposure. They form the central part of individual volcanic systems, passing laterally to flow-banded facies, which represent the external and exposed parts of the system. These facies can be recognized in the inner part of a rhyolitic lava dome (Fig. 6C).

The massive facies are medium- to fine-grained and show a porphyritic texture with crystal aggregates composed of K-feldspar, biotite, amphibole, and

quartz immersed in a felsitic groundmass. Accessory minerals are zircon, apatite, and magnetite. Static recrystallization of the groundmass can be recognized in some of the samples (Fig. 6D).

Eruptive fissures are defined as dilatational cracks that emit lavas, while dykes and sheet-like intrusions are the subsurface equivalents. These intrusions may contain tens to hundreds of members (Walker, 1999). Dykes and eruptive fissures correspond to coherent facies. Dykes are fine- to medium-grained, pale orange, and rhyolitic to rhyodacitic in composition, with porphyritic and microgranular textures indicating two different types of emplacement.

The porphyritic facies form sheet-like and rounded small bodies of 0.1–2 km in length and 1 to 50 m thick, without thickness variations along the strike. They consist of quartz, K-feldspar, amphibole, biotite, and scarce plagioclase. Accessory minerals are magnetite, zircon, and apatite. Microgranular facies are minor and are formed by quartz, plagioclase, K-feldspar, and scarce hornblende and biotite. Quartz phenocrysts show straight to curved edges and reach 3 mm in size. Some specimens have irregular shapes and undulose extinction. Myrmekitic textures are common.

The jigsaw breccia facies are formed by 6 to 20 cm long subangular to angular fragments of rhyolitic composition of the massive and flow-banded facies (Fig. 6E). A feature of this facies is that individual fragments are closely juxtaposed with an absence of marked displacements in between. As indicated above, this facies is always associated with the massive and flow-banded rhyolitic facies.

Both, the massive and flow-banded rhyolites (Lithofacies VI and VII) were interpreted as forming the internal and coherent parts of lavas, lava domes, and synvolcanic dykes (McPhie et al., 1993).

3.2. Geochronology

In order to obtain a precise age of the Garamilla volcanic unit in this area, one sample of the initial volcanic activity (sample DN4) was obtained from a dacitic lapilli-tuff located at 40°15'40"S and 69°5 7'35"W. From that, 33 zircon grains were recovered and analyzed for geochronology at the Arizona LaserChron Center, Department of Geosciences, University of Arizona, using the procedures described by Gehrels et al. (2008).

The zircons observed are typically fine- to medium-grained (70–250 μm long), and show euhedral morphology with magmatic zonation, with preserved faces and interfacial edges. No overgrowths or metamorphic zircons with internal structures were observed. Thirty zircon analyses showed moderate U values (108–655 ppm), while the other three presented low U values (37–98 ppm).The high Th/U values are consistent with a magmatic origin (>0.5).

The data form a unimodal zircon distribution (Fig.7A) comparable with the previously obtained age in the Quiñenao area (Benedini and Gregori, 2013), with a main population crystallizing between 186 and 197Ma (82.06%) and a main peak at 190Ma. Two smaller population grain ages are recognized, the younger one belonging to Upper Carboniferous–Lower Permian with ages of between 270 and 304 Ma (10.25%) and the oldest one (7.69%) revealing Upper Silurian rocks in the source area.

Figure 7B shows the results of the U-Pb geochronological analysis of a dacitic Lapilli-tuffs sample (DN4) in a concordia diagram (details in Table 1). The ages of individual zircon grains show a range of dispersion from 186 to 420 Ma. A total of 33 analyses were plotted in the concordia line and discordant ages were not recorded. The concordia age is 188 ± 0.64 Ma with a mean square weighted deviation (MSWD) of 0.033 and a concordance probability of 0.85.The weighted average shown in Figure 7C reveals a mean age of 189± 0.76 Ma, with two rejected data. MSWD is 0.88 with 0.65 probability. We interpreted the final value (189 Ma) as the timing of the magmatic crystallization of the zircons and the deposition of the dacitic lapilli-tuff facies.

3.3. Geochemical analyses

Preliminary geochemistry was performed in terms of characterizing and correlating the volcanic unit studied with similar units previously characterized by Pankhurst and Rapela (1995), D´Elia et al.(2012), and Benedini and Gregori (2012). Twelve samples from Lithofacies III to VIII were analyzed for major, trace, and rare earth elements following the procedures used in ACTLAB (Table 2) using XRF and INAA. In pyroclastic rocks, carefully separation of lithic fragments was done. Seven samples showed low loss of ignition varying from 0.7% to 1.5%, with five samples above 1.8%. It was verified that many elements, such as Sm, Nb, Th, U, Rb, and Pb, exhibit a positive correlation with Zr, suggesting that low-T alteration did not significantly affect the elemental or isotopic compositions of the rocks.

3.3.1. Major elements

The major element contents reveal a high potassium calc-alkaline tendency for the pyroclastic sequence and dykes (Peccerillo and Taylor, 1976; Fig.8A) with K_2O concentrations ranging from 2.84 to 4.95%. SiO_2, on the other hand, varies between 66% and 78% (Lithofacies I was not analyzed). However, this wide range is dominated by compositions with SiO_2 higher than 70%. According to the abundance of K_2O and Na_2O vs. silica diagram (Le Bas et al., 1986), the samples are dacitic and rhyolitic in composition (Fig. 8B). The MgO values reach 1.17% in the eutaxitic lapilli-tuffs of dacitic composition, whereas Fe_2O_3 reach 4.13% in the lesser differentiated facies. These features indicate highly differentiated magmas.

According to the Cox et al. (1979) diagram (Fig.8C), the rocks are classified as dacites and rhyolites. The Al_2O_3 content varies between 11.23% and 15.02%. Eleven samples (91%) were plotted as peraluminous, while the initial deposits (eutaxitic lapilli-tuffs of dacitic composition) show a metaluminous character (Shand, 1951). All the analyzed samples display a calc-alkaline tendency with the initial volcanic event located away from the alkali corner in the Irvine and Baragar (1971) diagram (Fig. 8D), moving to the alkali corner in the more evolved facies, which is consistent with alkaline rhyolites (Fig. 8E). According to the Streckeisen (1976) diagram, rocks range from dacites to alkaline rhyolites, with four samples of acidic dykes being alkaline rhyolites.

3.3.2. Trace elements

The rocks classified according to the SiO_2 versus Zr/TiO_2 and Zr/Ti versus Nb/Y diagrams of Winchester and Floyd (1977) confirm dacitic and rhyolitic

compositions (Figs. 9A and B).Values lower than a 0.6 Nb/Y ratio indicate that they belong to the subalkaline series. On the chondrite-normalized expanded diagrams (Thompson, 1982) of Fig. 9C, the distribution of trace elements shows enrichment in large-ion lithophile elements (LILE; Ba, Rb, Th, K, Sr, La, Ce) and the depletion of Sr, P, and Ti. The acidic dyke facies generally have more significant negative anomalies in Ti, P, and Sr, and higher concentrations of LILE, indicating the fractionation of apatite and titanite during magmatic evolution with enrichment in K-feldspar. These patterns are consistent with the samples analyzed in Quiñenao area and assigned to the Garamilla Formation (Benedini and Gregori, 2013).

The Zr concentrations range between 54 and 257 ppm and show an inverse relationship with the SiO_2 concentrations. Another feature shown in Fig. 9C is the negative anomaly of Nb and Ta relative to Th and La, which is typically considered to be a signature of a subduction zone involved in the petrogenetic process, in which Nb and Ta do not dissolve in melts derived from the descending plate, producing anomalous depletion in arc-related magmas (Sun, 1982).The LILE enrichment also suggests that the source magma has received contributions from fluids derived from a subducted oceanic crust.

3.3.3. Rare earth elements

The samples analyzed present total REE concentrations ranging from 102 to 190 ppm, and patterns enriched in light rare earth elements (LREE) and depleted in heavy rare earth elements (HREE) in chondrite-normalized diagrams (Sun and McDonough, 1989). Nearly all samples show moderate negative Eu anomalies (2.04–0.53) associated with fractionation of plagioclase.

In all samples, enrichment of LREE and similar slopes (La_N/Lu_N) indicate the cogenetic character of the rocks. Medium rare earth elements (MREE) and HREE values are consistent with hornblende fractionation and the absence of garnet in the parental magma (Fig. 9D).

The ratio of Ta to Yb (0.19–0.95) also shows igneous environments related to convergent plate margins (volcanic arc; Pearce, 1982).The diagram Th/Yb vs Ta/Yb (Pearce, 1983; Fig 9E) indicates the shoshonitic signature of the analyzed samples, with a within-plate evolution even for the less evolved members. Samples of the Quiñenao area (Benedini and Gregori, 2013) were also included for comparison.

The studied rocks were plotted also on the Nb versus Y diagram (Pearce et al., 1984). The samples are grouped (Fig. 9F) in the field of magmatic arc-related rocks.

3.4. Structural analysis: dyke attitude

Three curved swarms of dykes, probably of Jurassic age, cover almost 800 km^2 in the western sector of the North Patagonian Massif (40°10' S to 40°23' S and 69°42' W to 70°02' W; see Figs. 10 a nd 13).The acidic dykes separate three complexes from one another by 4–6 km: South Complex (I), Central Complex (II), and North Complex (III).

The South Complex (I) is located near the Cerro Carro Quebrado and Cerro Pafaniyeu and extends westward through the Limay River entering the Neuquén Province. In the western sector of this complex we measured the strike and dip of 37 dykes. The average strike in this area is N 90–96°with dips of 70–80°to the north (Fig. 10, rose diagram I). E astwards, the strike

progressively changes to the main direction of N 112°, with a dip mainly to the NE (diagram II). The eastern portion of this system reveals an increasing structural complexity with two principal domains: one dominated by a N115° strike with dips mainly to the NE, and the second with strikes at N193° dipping to the SE (Fig. 10, diagram III). The preliminary hypothesis is that extension direction changes from a N–S to a NE–SW direction.

The central complex is located 1.5 km south of Cerro Guacho and 2.3 km south of Cerro Catri Cura. Its westernmost outcrops reach the Limay River, while eastward it extends in the direction N 115° for more than 9 km. Here, the main population (Fig. 10, diagram IV) follows a N120° strike, with dips (71°) to the SW. The easternmost part also displays a more complex design related to the presence of dykes that are nearly N–S. In this belt, the maximum stretching strain seems to be located in a NE–SW direction.

The northern complex starts northeast of the Piedra del Aguila dam, ending nearly at Cañadón Blancura. In the first locality, strikes are predominantly E–W, whereas eastwards they change to N140° with dips to the SW (Fig. 10, diagram V), and N160° with dips to the SW (Fig. 10, diagram VI). In this area another population of dykes appears with strikes N20°. Here, the stretching strain is in a NE–SW direction, as observed in the other complexes, and is partly coincident with the circumferential dyke system described by Benedini and Gregori (2013).

The dyke swarm described above resembles the fault pattern developed on the margins and floor of a highly oblique rift, as shown by several authors (Agostini et al., 2009; Autin et al., 2010; Corti, 2012).

4. Discussion

4.1. Facies interpretation

4.1.1. Stage 1

This stage is formed by flow banded andesites that developed mainly in the southern area and erupted directly over the Mamil Choique Formation. They are covered by massive lithic breccias, indicating the beginning of the volcanic system (Fig. 11). This stage must be pre-Pliensbachian and possibly related to dilatational zones (Fig. 12).

4.1.2. Stage 2

The onset of the eruption is marked by the basal massive lithic breccias (Fig. 11). The development of these coarse deposits has been restricted due to a strong topographic control. Their limited distribution is interpreted as the product of explosive eruption through the pre-existing rocks. The homogeneity of the underlying country rock, mainly formed by granites, gives this facies a monolithologic composition. This facies can be interpreted as the collapse of the volcanic caldera (Lithofacies II and III).

The facies exhibit an asymmetrical, half-moon distribution, mainly located in the southeastern part of figure 12, which we interpret as a differential subsidence rate in the volcanic caldera.

Progressive vent opening is represented by a change in size, concentration, and composition of the lithic fragment, which changes to a lithic-rich ignimbrite, as mentioned. A marked fining upwards grading in this deposit can be interpreted as the waning current deposition. The progressive dilation of a conduit or decrease of the volatiles can produce eruptive waning (Branney

and Kokelar, 2002).This stage can be related to vent opening during the initial collapse of the volcanic system.

4.1.3. Stage 3

This stage of the eruption involves Lithofacies IV, representing an increase in the magma discharge rate, composed of the voluminous, coarse-crystal rich massive lava-like ignimbrites. This stage is represented by multiple, steady eruptions of lithic-poor pyroclastic flow deposits as the eruption waned and stabilized. This lithofacies has the greatest volume and lateral distribution, and is considered the principal in-filling deposit (Fig. 12).

The vertical arrangement of this pyroclastic unit suggests a multiple discharge eruption for this stage that seems to progress from the SE area. Locally, at the base of some of these flows appear fine-grained deposits that can be interpreted as 2b-type ignimbrite deposits, according to Sparks (1976).

In other areas a non conformity appears between this stage and stage II, as indicated in paragraph 3.1.4 and represented in Fig. 3E, indicative of the subsidence development. The greatest volume of this lithofacies erupted apparently in a relatively short period and the absence of sedimentary rocks in the inner part of the caldera indicates a rapid subsidence and collapse of the caldera floor.

Later, there is evidence of a waning stage in the volcanic evolution, which is preserved in small volume fine-crystal rich eutaxitic lapilli-tuffs (Lithofacies V) developed in the margins of the volcanic structure.

This volcanic stage can be divided into an initial pulse, which is more volumetric and represented by Lithofacies IV, and a final pulse constituted by

the rocks of Lithofacies V, with minor relevance and less development than the first one. The initial pulse is better represented in the central area of the volcanic structure. The field and microscopic characteristics that allow both pulses to be distinguished are: (1) a sharp and recognizable contact between both pulses, (2) mesoscopic eutaxitic textures in the second pulse, and (3) the first pulse occupies the central area of the volcanic system, whereas the second appears mostly in the margins.

4.1.4. Stage 4

This stage is represented by Lithofacies VI, VII, and VIII of rhyolitic composition, which mainly form lava flows, lava domes, and dykes. Lavas and lava domes present a sub-circular distribution in the southeastern part of the area, which is considered to be the border or margin of the depocenter or caldera (Fig. 12). Its distribution, which can be observed in Fig. 5, is coherent with the outcrop of rocks belonging to stage 2, which were interpreted as the initial stage of collapse.

Because these rocks are mainly effusive and occur at a later collapse stage, it is considered that they were erupted at post-collapse due to depressurization of the magmatic chamber. The absence of gravity-collapsed pyroclastic deposits associated with the above-mentioned bodies allows us to suppose the endogenous growth of them. Therefore, stage IV is considered to be a post-collapse stage of volcanism (Fig. 12).

Dykes consisting of tabular bodies contrast partly with those cited above. Here, there are mostly dacitic to rhyolitic dykes, and due to their geochemistry

and field relationships with the pyroclastic sequence, they can be included in the Garamilla Formation.

Their geographical distribution widely exceeds the outcrops of the Garamilla Formation, indicating that the development of this system could have been promoted by the early structures of the host rocks, a generalized extension in this area, and the existence of a magmatic chamber.

The dyke swarm displays an en-echelon arrangement formed by three systems, as described in paragraph 3.4. This type of arrangement is frequently mentioned in order to explain the regional stress in rifting zones, such as Iceland, East Africa, and New Zealand, where mantle plumes and continental rifting are invoked to explain volcanic systems (Corti, 2012). According to Pollard and Segal (1987) and Rubin (1995) dyke advance is driven by the internal pressure of the melt, which results in the brittle dilation of the surrounding media. Crack propagation direction is determined by the orientation of the stress, and the dyke walls are assumed to be normal to the least compressive stress.

4.2. Geometry of dyke arrays

As indicated in 3.4, three curved swarms of dykes have been described in the western sector of the North Patagonian Massif. These swarms of dykes show a pseudo-parallel design in their western part with strikes from N90° to N115°, and a more complex eastern part with nearly N–S strikes. In this part, an en-echelon system appears with strikes from N120° to N160° (Fig. 13 A). Finally, in this area a N190° system appears. This system is mainly composed of basic dykes. Their strikes, which are nearly parallel to the extensional strain,

indicate that they were developed in another stress system, previous to the Jurassic regime (Fig. 13A).

The entire complex of Jurassic dykes resembles the fault pattern developed in the floor of a highly oblique rift, as showed by several authors (Agostini et al., 2009; Autin et al., 2010; Corti, 2012) and represented in the model in Fig. 13B. There, the dyke complex seems to be intruded in preexisting fractures zones configuring (1) en-echelon, border faults, (2) internal curved (roughly extension-orthogonal) faults, and (3) rift-parallel faults.

Fig. 13B, from Agostini et al., (2009) and Corti (2012) represents a experimental model of the beginning of the extension of a highly oblique rift. According Agostini et al., (2009) the model represents a reasonable approximation of the natural process of continental rifting at a regional scale, where extensional stresses are applied to a predeformed, anisotropic lithosphere and deformation is not randomly distributed but tends to follow the trend of preexisting weaknesses inherited from previous deformation phases avoiding stronger regions.

Considering an initial extension of the model equivalent to 13.5 km, en-echelon, border faults and rift-parallel faults are not developed.

As the extension progresses (Fig. 13C) to an equivalent of 40.5 km, rift-parallel faults and en-echelon, border faults appear. In our particular case, that can be considered as intermediate stage, the swarm of dykes described can be interpreted as internal curved faults, roughly orthogonal to the extension.

The highly and moderately oblique rifts (α: 40–60°) are usually associated with a complex design of faults and fractures. Corti (2012) suggested that the rheological limits of the highly oblique rift system are nearly parallel to the

extension. This author also indicated that floor subsidence in these rifts is less important than in low oblique rifts where α increases considerably. Accordingly with the above mentioned, the existence of highly oblique rifts with a principal extensional strain in a NNE–SSW direction (~N10°) in the area located at 40° 10' S to 40°23' S and 69°42' W to 70°02' W cannot be ruled out. Inside this structure, the pseudo-parallel complexes of dykes are nearly orthogonal to the extension, whereas the en-echelon dykes, developed in the eastern part, must be related to the rift borders, which are NW–SE directed.

The relationships between volcanic activity and the amount of extension was extensively analyzed by Spinks et al. (2005) at Taupo, who recognized that segments with major extension are associated with significant volumes of volcanic rocks. In portions where the shear component of the stress system is predominant, small amounts of volcanic rocks were recognized. Furthermore, in our study area major ratios of extension, located in the western part of the system, are occupied by collapsed volcanic systems of rhyolitic composition.

4.3. Geochemical constraints

The Garamilla Formation is composed predominantly of pyroclastic and volcanic rocks of a high-potassium calk-alkaline series. They represent nearly 95% of the rocks. The silica content gradually increase from an initial dacitic-andesitic-dominated magma to a medium–high concentration of silica (dacites and rhyolites), which progressively increases along with the content of alkali. The effusive, more evolved members (dykes) are linked to the alkaline series suggesting that batches of new magma were not added.

The MREE and HREE values are consistent with hornblende and biotite fractionation together with the absence of garnet in the parental magma, which is indicative of the hydrated nature of these magmas.

The distribution of the trace and rare earth elements in the chondrite and MORB-normalized diagrams shows an evident negative depletion of Nb with respect to other elements. This feature is interpreted as evidence of subduction components. However, such a consideration is valid for those rocks in which the subduction environment can be set independently (Roberts and Clemens, 1993).

Another feature in these multi-element diagrams is the co-genetic character of all the lithologies. A progressive development of a negative Eu anomaly is related to an increase of alkalis and silica, indicating an augmentation of the fractionation of plagioclase. This behavior coincides with the intraplate trend represented in the Th/Yb vs. Ta/Yb diagram, which suggests relatively long periods of magma residence in the crust.

This feature may be related to the significant thickness of the crust in the western part of the Río Negro Province, which is constituted mainly by a major batholith of Permian age (Mamil Choique Formation) together with gneisses and migmatites of the Silurian–Devonian age.

Experimental data on partial melting of crustal rocks developed by Roberts and Clemens (1993) suggest that high potassium I-type magmas occur in different geotectonic environments, but can only be derived by partial melting of calk-alkaline metamorphic rocks or mafic to intermediate calk-alkaline high-potassium rocks.

4.4. Correlation with units in the Neuquén Basin

As indicated by several authors (Gulisano et al.,1984; Veiga et al.,1999; Cristallini et al.,2006, 2008, 2009; Silvestro and Zubiri, 2008; Pángaro et al. 2008 and references therein), in the northeastern border of the Neuquén basin the Late Triassic–Sinemurian rifting episode (Mombrú and Ulliana, 1978, Vergani et al. 1995), is represented by half-graben structures.

According Silvestro and Zubiri, (2008), the principal population are wide and deep grabens that strike >N130°, whereas the se cond population are narrow and shallow grabens striking <N110°. The geo metry of these two graben populations was explained by Silvestro and Zubiri, (2008), as due to a NW to SE-directed compression, that produce the oblique convergence between a rigid block located south (North Patagonian Massif) and the Neuquén Basin located north.

Most of the half-graben structures contain continental and volcaniclastic sequences, known as the Precuyano Cycle (Gulisano et al., 1984). For Vergani et al. (1995) the change to the marine facies of the Cuyo Group (Pliensbachian-Callovian) is indicated by a Lower Pliensbachian unconformity. Vergani et al. (1995) also suggested that the Cuyo Group depocenters were controlled by the pre-existent Late Triassic–Sinemurian half-graben structures.

In the southeastern border of the basin both strike directions were recognized in the Quiñenao area (Benedini and Gregori, 2013) and in the Cerro Carro Quebrado and Cerro Catri Cura area. In particular, the Precuyano Cycle (Sañicó Formation) cropping out 7 km westwards of our studied area is temporary and geochemically correlatable with the Garamilla Formation.

The timing of the eruption of the dacitic lapilli-tuffs of the second eruptive unit of the Garamilla Formation in the Quiñenao area was established by a $^{206}Pb/^{238}U$ age of 187 ± 2.3 Ma (MSWD: 0.4). The age obtained in the Cerro Carro Quebrado and Cerro Catri Cura area of 189± 0.76 Ma ($^{206}Pb/^{238}U$) is in agreement with the above cited age.

The Sañicó Formation represents a calc-alkaline series (D'Elia et al., 2012), but because more than 50% of the sequence are differentiated acidic rocks, the unit is not completely comparable with a normal volcanic arc series.

The geochemistry of the Garamilla Formation in the Cerro Carro Quebrado and Cerro Catri Cura area strongly resembles the results of Schiuma and Llambías (2008) and Bermúdez et al. (2002) for rocks that can be related to the Precuyano Cycle rocks located in the subsurface north of the Huincul Fault Zone and Anticlinal Campamento, in the central part of the Neuquén Basin.

Their results are also compatible with those of Benedini and Gregori (2013) for the Garamilla Formation in the Quiñenao area, indicating that Lower Jurassic magmatism was widespread in the Neuquén Basin

4.5. Geological setting and correlation with units in the North Patagonian Massif and the North Patagonian Cordillera

Dalziel et al. (1987) and Uliana et al. (1989) showed evidence for the development of extensional basins in Argentina and Chile during the Jurassic and Triassic respectively. Uliana et al. (1989) indicated that these basins are sub-parallel, roughly along NNW–SSE trends, and are inferred to be controlled by the reactivation of older Paleozoic NW and NE-striking structures.

According to Martin et al. (1999), in the 35–39°S region of Chile, during the Middle Permian to Middle Jurassic, occurred the cessation of Late Paleozoic subduction-related magmatism. During this time span, the volcanic and sedimentary sequences record the transition between transpressional deformation, associated with oblique convergence along the margin, and extension along the Gondwana margin.

Furthermore, Kay et al. (1989) have suggested that the Late Paleozoic–Jurassic silicic magmatism erupted at the southwestern margin of Gondwana—South America—was formed in an extensional setting without subduction. However, in the area located southwest of this study, in the North Patagonian Cordillera, between 41°30´ and 45°S, Gordon and O rt (1993) and Haller et al. (1999) described the Subcordilleran Patagonian Batholith or the Subcordilleran Plutonic Belt, composed of granitic and volcanic rocks of Jurassic age. Rapela et al. (2005) have shown that the granitic rocks in this plutonic belt have SHRIMP U-Pb ages between 181 ± 2 Ma and 185 ± 2 Ma. Further north, in the Puelo-Lacar lakes (40°10´ to 42°S), the Montes de Oca Formation and the Huemul Group (González Bonorino, 1974), is composed of dacites and andesites that can be assigned to an arc-related volcanism. The rocks were K-Ar dated by González Díaz (1982), who yielded tentative ages between 120 and 155 Ma, discarding up to now a correlation between the Huemul Group and the rocks here studied.

The other arc-related unit is Nacientes del Bio Bio Formation, described in the North Patagonian Cordillera between 38°and 39° S. There, De la Cruz and Suárez (1997) established the existence of submarine tholeiitic basalts, with intercalated turbidites, of island arc affinities (Icalma Member). The presence of

harpoceratides *Paltarpites ?, Harpoceras ?* and *Atacamiceras?* indicates a Late Pliensbachian to Early Toarcian age (183–178 Ma),

The data presented by Rapela et al. (2005) demonstrated that the magmatism in the Subcordilleran Plutonic Belt was coincident with the acidic magmatism of the Marifil Complex (North Patagonian Massif). This unit is represented by 2.5 km thickness of ignimbrites, domes, and pyroclastic rocks considered as linked to a crystal fractionation from a parental andesitic magma during partial melting of a mafic lower crust (Pankhurst and Rapela, 1995).

According to Pankhurst et al. (2000), the rhyolites of phase 1 of the volcanism (188–178 Ma, Marifil Complex) show a within-plate geochemical signature.

The ages of the Garamilla Formation (189± 0.76 Ma -187 ± 2.3 Ma, this paper and by Benedini and Gregori 2013) are in the range of the ages of phase 1 of the volcanism (188–178 Ma, Marifil Complex) recognized by Pankhurst et al. (2000) in Patagonia.

The geochemical signatures of the Garamilla Formation in the Cerro Carro Quebrado and Cerro Catri Cura areas do not fulfill those of the classical subduction-related volcanic arcs, and the strong chemical similarity with the Marifil Complex suggests an intraplate setting for the Garamilla Formation.

Therefore, our interpretation favors an intraplate setting of the emplacement of the volcanic rocks of the Garamilla Formation in this area related to the extensional conditions that prevailed during the development of the acidic volcanism.

5. CONCLUSIONS

The Garamilla Formation studied in the Cerro Carro Quebrado and Cerro Catri Cura area, located in the west region of the Río Negro Massif, is composed of four volcanic stages: andesitic lava-flows related to the beginning of the volcanic system; basal massive lithic breccias that represent the caldera collapse; voluminous, coarse-crystal rich massive lava-like ignimbrites related to multiple, steady eruptions that represent the principal infill of the system; and, finally domes, dykes, lava flows, and lava domes of rhyolitic composition indicative of a post-collapse stage.

A dyke complex, formed by three braches was recognized during this work. The regional design of these branches is considered as formed in high-obliquity rift systems due to curved pattern comparable to floor fractures developed in such extensional systems. The analysis of the above mentioned structural evidences, as well as, the architectures of the volcanic facies, such as sub-circular arrangements indicate that the existence of a highly oblique rift where the volcanic system was emplaced. The highly oblique rift seems to be controlled by a principal extensional strain in a NNE–SSW direction (~N10°), as in the Neuquén Basin.

The rocks belonging to this volcanic system are mainly high-potassium dacites and rhyolites, with trace and RE elements contents coincident with intraplate signatures as recorded in the Marifil Complex. This unit is represented by a 2.5 km thick sequence of ignimbrites, domes, and pyroclastic rocks related to intraplate magmatism.

The age obtained in the Cerro Carro Quebrado and Cerro Catri Cura area (189± 0.76 Ma) agrees with those obtained in the Quiñenao area, as well as in

the Neuquén Basin, indicating that the Lower Jurassic magmatism was widespread in the western area of the North Patagonian Massif and in the Neuquén Basin. The age is also coincident with the phase 1 of volcanism in Patagonia (188–178 Ma, Marifil Complex) of the eastern North Patagonia Massif.

Acknowledgments

This study is part of the PhD of Leonardo Benedini, granted by research projects, entitled *Configuración Gondwánica del sector occidental de la Comarca Nordpatagónica, Argentina*, Pict BID 2007 N 01649, FONCYT, and *Configuración geológica y geodinámica del sector central de la Comarca Nordpatagónica, Argentina* (24/H100), Universidad Nacional del Sur.

We would like to thank Gastón Alvarez and Dr. Sergio Delpino for helping during field trips and fruitful discussions about the petrology of the Garamilla Formation. Many thanks to the Arias and Cortes families, as well as to the Mapuche communities of Blancura Centro and Rincón Chico that allowed us access to their lands, gave us shelter, and helped throughout the many field trips.

Constructive and thoughtful reviews by Dr. I. Petrinovic, an anonymous colleague and Dr. V Ramos on the early version of this manuscript greatly improved the same, for which we are truly grateful.

References

Agostini, A., Corti, G., Zeoli, A., Mulugeta, G., 2009. Evolution, pattern and partitioning of deformation during oblique continental rifting: inferences from lithospheric-scale centrifuge models. Geochemistry, Geosphysics, Geosystems (GCubed) 10, Q11015. doi:10.1029/2009GC002676

Allen, R. L., Cas R. F. A. The Rosebery controversy: distinguinshing prospective submarine ignimbrite-like units from true subaerial ignimbrites in Rosebery-Hercules ZnCuPb massive sulphide district, Tasmania. Geological Society Australia, Abs 25, 31-32

Alric, V.I., Haller, M.J., Feraud, G., Bertrand, H., Zubia, M., 1996. Cronología $^{40}Ar/^{39}Ar$ del Volcanismo Jurásico de la Patagonia Extrandina. Actas 13 Congreso Geológico Argentino, 5, 243–250.

Autin, J., Bellahsen, N., Husson, L., Beslier, M.O., Leroy, S., d'Acremont, E., 2010. Analogue models of oblique rifting in a cold lithosphere. Tectonics 29, TC6016. doi:10.1029/ 2010TC002671.

Benedini, L., Gregori, D.A., 2012. La Formación Garamilla: evento volcánico del Jurásico Inferior del sector occidental de la Comarca Nordpatagónica, Provincia de Río Negro, Argentina. Aportes al Magmatismo y Metalogénesis. Serie Correlación Geológica, 28, pp. 9–26. San Miguel de Tucumán.

Benedini, L., Gregori, D., 2013. Significance of the Early Jurassic Garamilla formation in the western Nordpatagonian Massif. Journal of South American Earth Sciences, 45, 259–277.

Bermúdez, A., Delpino, D., Pángaro, F., 2002. Volcanismo de arco asociado a procesos de subducción e extensión durante el Triásico Superior e Jurásico Inferior (Precuyano). Área Cerro Bandera, Cuenca Neuquina, Argentina. In: 4 Congreso de Exploración y Desarrollo en Hidrocarburos, Actas en CD. Mar del Plata.

Branney, M.J., Kokelaar, P., 2002. Pyroclastic density currents and the sedimentation of ignimbrites. Geological Society, London, Memoir, 27, 143 pp

Branney M. J. Sparks R. S. J., 1990. Fiamme formed by Diagenesis and burial compactacion in soils and subaqueous sediments. Journal of Geological Society of London 147: 919-922.

Cas, R. A. F.; Wright, J. W., 1987. Volcanic successions: Modern and ancient. Chapman and Hall. Londres, 528 pp

Cortés, J.M., 1981. El sustrato precretácico del extremo nordeste de la provincia del Chubut. Revista de la Asociación Geológica Argentina 36, 3, 217-235.

Corti, G., 2012. Evolution and characteristics of continental rifting: analogue modeling-inspired view and comparison with examples from the East African Rift System. Tectonophysics, 522-523, 1-33

Cox, K.G., Bell, J.D., Pankhurst, R.J., 1979. The interpretation of igneous rocks. Allen and Unwin, London. 450 pp.

Cristallini, E.O., Bottesi, G., Gavarrino, A., Rodriguez, L., Tomezzoli, R.N., Comeron, R., 2006. Synrift geometry of the Neuquén Basin in the northeastern Neuquén Province, Argentina. In: Kay, S.M. and Ramos, V.A. (Eds.) Evolution of the Andean margin: a tectonic and magmatic view from the Andes to the Neuquén Basin (35°-39° S lat). Geological Society o f America Special Paper 407, 147-161.

Cristallini, E., Pando, G., Martínez, J. M., Buhler, M., Tomezzoli, R., Barredo, S., Zambrano, O., 2008. Controles precuyanos en la estructura de la cuenca Neuquina. 17 Congreso Geológico Argentino (Jujuy), Actas 2, 759-760.

Cristallini, E., Tomezzoli, R., Pando, G., Gazzera, C., Martínez, J. M., Quiroga., J., Buhler, M., Bechis, F., Barredo, S., Zambrano, Z., 2009. Controles precuyanos en la estructura de la cuenca neuquina. Revista de la Asociación Geológica Argentina 65, 2, 248-264.

Cúneo,' R., Ramezani,' J., Scasso,' R., Pol d., Escapa, I., Zavattieri A.' Bowring S. A.. 2013. High-precision U–Pb geochronology and a new chronostratigraphy for the Cañadón Asfalto Basin, Chubut, central Patagonia: Implications for

terrestrial faunal and floral evolution in Jurassic, Gondwana Research, 24, 3–4, 1267–1275.

Dalziel, I. W. D., Storey, B. C., Garrett, S. W., Grunow, A. M., Herrod, L. D. B., Pankhurst, R. J., 1987. Extensional tectonics and the fragmentation of Gondwana. In: Coward, M.P. (Ed.) Continental Extensional Tectonics, Geological Society Special Publication 28, 433-441, London.

De la Cruz, R., Suárez, M., 1997. El Jurásico de la cuenca de Neuquén en Lonquimay y Chile. : Formación Nacientes del Biobio. (38-39° S). Revista Geológica de Chile, 24, 1, 3-24.

D'Elia, L., Muravchik, M., Franzese, J. R., Bilmes, A., 2012. Volcanismo de sinrift de la Cuenca Neuquina, Argentina: relación con la evolución Triásico Tardía-Jurásico Temprano del margen andino. Andean Geology, 39, 1, 106–132.

Escapa, I., Cúneo, R., Cladera, G., 2008. New evidence for the age of the Jurassic flora from Cañadón del Zaino, Sierra de Taquetrén, Chubut. Ameghiniana 45, 633–637.

Franzese, J. R., Pankhurst, R. J., Rapela, C. W., Spalletti, L. A., Fanning, M., Muravchik, M., 2002. Nuevas evidencias geocronológicas sobre el magmatismo

Gondwánico en el noroeste del Macizo Nordpatagónico. 15 Congreso Geológico Argentino, Actas en CD, El Calafate.

Féraud, G., Alric, B., Fornari, M., Bertrand, H., Haller, M., 1999. 40Ar/39Ar dating of the Jurassic volcanic province of Patagonia: migrating magmatism related to Gondwana break-up and subduction. Earth and Planetary Science Letter, 172, 83-96.

Gehrels, G. E., Valencia, V. A., Ruiz, J., 2008. Enhanced precision, accuracy, efficiency, and spatial resolution of U-Pb ages by laser ablation–multicollector–inductively coupled plasma–mass spectrometry: Geochemistry, Geophysics Geosystems, Q03017, doi: 10.1029/2007GC001805.

González Bonorino, F., 1974. La Formación Millaqueo y la Serie porfirítica de la Cordillera Nordpatagónica: Nota preliminar. Revista de la Asociación Geológica Argentina 29, 145-154.

González Díaz, E. F., 1982. Zonación cronológica del plutonismo en los Andes Patagónicos septentrionales entre los 40‟00´y 42°0 0 sur: La migración de los ciclos intrusivos. Acta Geológica Lilloana, 16, 1, 5-22

Gordon, A., Ort, M. H., 1993. Edad y correlación del plutonismo subcordillerano en las provincias de Rio Negro y Chubut (41°-42°30´ L.S.). 12 Congreso Geológico Argentino, Mendoza, Actas 4, 120-127.

Gregori, D.A., Kostadinoff, J., Strazzere, L., Raniolo, A., 2008. Tectonic significance and consequences of the Gondwanide orogeny in northern Patagonia, Argentina. Gondwana Research 14, 429-450.

Gulisano, C. A., Gutiérrez Pleimling, A., Digregorio, R., 1984. Esquema estratigráfico de la secuencia jurásica del oeste de la provincia del Neuquén. 9 Congreso Geológico Argentino, Actas 1: 236-259. Buenos Aires.

Haller, M. J., Linares, M., Ostera, H. A. and Page, S. M. 1999. Petrology and geochronology of the Subcordilleran Plutonic Belt of Patagonia Argentina. 2 South American Symposium on Isotope Geology, Carlos Paz, Argentina, Actas, SEGEMAR, Buenos Aires, 210-214.

International Commission on Stratigraphy, 2009. International Stratigraphic Chart.

Irvine, T. N., Baragar, W. R., 1971. A guide to the chemical classification of the common igneous rocks. Canadian Journal of Earth Sciences 8, 523–548.

Kay, S. M., Ramos, V. A., Mpodozis, C., Sruoga, P. 1989. Late Palaeozoic to Jurassic silicic magmatism at the Gondwana margin: Analogy to the middle Proterozoic in North America? Geology 17, 324-328.

Le Bas, M. J., Le Maitre, R. W., Streckeisen, A., Zanettin, B., 1986. A chemical classification of volcanic rocks based on the total alkali-silica diagram. Journal of Petrology, 27, 745–750.

Lesta, P., Ferello, R., 1972. Región extrandina de Chubut y norte de Santa Cruz. In: Leanza, A.F., (Ed.), Geología Regional Argentina, Academia Nacional de Ciencias, Córdoba. pp. 601-687.

Lizuaín, A. Silva Nieto, D. 2005. Observaciones Geológicas en la región de Río Chico, Gastre, río Chubut Medio, provincia del Chubut. 16 Congreso Geológico Argentino (La Plata), Actas 1: 133-139.

Malvicini, L., Llambías, E., 1974. Geología y génesis del depósito de manganeso Arroyo Verde, provincia del Chubut. 5º Congreso Geológico Argentino, Actas 2: 185-202.

Martin, M. W, Kato, T. T., Rodriguez, C., Godoy, E., Duhart, P., McDonough, M., Campos, A., 1999. Evolution of the late Paleozoic accretionary complex and overlying forearc-magmatic arc, south central Chile (38°-41°S): Constraints for the tectonic setting along the southwestern margin of Gondwana. Tectonics 18, 4, 582-605

Mc Phie, J., Doyle, M., Allen, R., 1993. Volcanic textures: A guide to the interpretation of textures in volcanic rocks. Tasmanian Government Printing Office, Tasmania, 198 pp.

Mombrú, C. A., Uliana, M. A. 1978. Esquema tectosedimentario de la cuenca mesozoica de Mendoza y Neuquén. 7 Congreso Geológico Argentino (Neuquén), Actas 2: 239-256.

Nullo, F., Proserpio, C. 1975. La Formación Taquetrén en Cañadón del Zaino (Chubut) y sus relaciones estratigráficas en el ámbito de la Patagonia, de acuerdo a la flora, República Argentina. Revista de la Asociación Geológica Argentina 30: 133-150.

Nullo, F., 1978. Descripción geológica de la Hoja 41dc, Lipetrén. Provincia de Río Negro. Boletín 158. Servicio Geológico Nacional, Buenos Aires, p. 88.

Orchuela, I. A., Ploszkiewicz, J. V., 1984. La Cuenca Neuquina. In: Ramos, V.A. (Ed.) Geología y Recursos Naturales de la provincia de Río Negro. Relatorio del IX Congreso Geológico Argentino. pp. 163-188. San Carlos de Bariloche.

Page, S., Page, R., 1999. Las diabasas y gabros del Jurásico de la Precordillera del Chubut. In: Caminos, R. (ed.) Geología Argentina. Subsecretaría de Minería de la Nación, Servicio Geológico Minero Argentino, Instituto de Geología y Recursos Minerales, Anales No. 29, 489-495.

Pángaro, F., Pereira, D. M., Micucci, E. 2008. El syn-rift del ámbito de la dorsal de Huincul, cuenca Neuquina: su evolución e impacto en el registro

estratigráfico del Jurásico. 17 Congreso Geológico Argentino (Jujuy), Actas 2, 789-790.

Pankhurst, R. J., Rapela, C. W., 1995, Production of Jurassic rhyolite by anatexis of the lower crust of Patagonia. Earth and Planetary Science Letters, 134, 23- 36.

Pankhurst, R. J., Riley, T. R., Kelley, S. Fanning, C. M., 2000. Episodic silicic volcanism in Patagonia and the Antarctic Peninsula: chronology of magmatism associated with the break-up of Gondwana. Journal of Petrology, 41, 605-625.

Pearce, J.A., 1982. Trace element characteristics of lavas from destructive plate boundaries. In: Thorpe, R.S. (Ed.). Andesites: Orogenic Andesites and related rocks. Wiley and Sons, New York, pp.525–554.

Pearce, J. A., 1983. Role of the sub-continental lithosphere in magma genesis at active continental margins. In: Hawkesworth, C.J., Norry, M.J. (Eds.), Continental basalts and mantle xenoliths. Shiva, Nantwich, pp. 230-249.

Pearce, J.A., Harris, N. B. W., Tindle, A.G., 1984.Trace element discrimination diagrams for the tectonic interpretation of granitic rocks. Journal of Petrology, 25, 956–983.

Peccerillo, A., Taylor. S. R., 1976. Geochemistry of Eocene calc-alkaline volcanic rocks from the Kastamonu area, northern Turkey. Contribution to Mineralogy and Petrology, 58, 63–81.

Pollard, D. D., Segal, P. 1987. Theoretical displacements and stresses near fractures in rock: with applications to faults, joints, veins, dikes and solution surfaces In: Fracture Mechanics of Rock, Atkinson, B.K. (Ed.), Academic Press Inc, London pp. 277–349.

Rapela, C. W., Pankhurst, R. J., Fanning, C. M., Hervé, F., 2005. Pacific subduction coeval with the Karoo mantle plume: the Early Jurassic Subcordilleran belt of northwestern Patagonia. Geological Society, London, Special Publications, 246; 217-239.

Rapela, C.W., Pankhurst, R.J., 1993. El volcanismo riolítico del noreste de la Patagonia: un evento meso-jurásico de corta duración y origen profundo. Actas 12 Congreso Geológico Argentino 4, 179–188.

Roberts M.P., Clemens J.D., 1993. Origin of high-potassium, calcalkaline, I-type granitoids. Geology 21, 825–828.

Rubin, A.M., 1995. Propagation of magma-filled cracks. Annual Review Planetary Sciences, 23: 287-336.

Schiuma, M., Llambías, E.J., 2008. New ages and chemical analysis on Lower Jurassic volcanism close to the Huincul High, Neuquén. Revista de la Asociación Geológica Argentina, 63. 4, 644-652.

Shand, S. J., 1951. Eruptive Rocks. Their genesis, composition, classification, and their relation to ore-deposits. Wiley and Sons, New York, p. 488.

Silva Nieto, D., Cabaleri, N., Salani, F., Coluccia, A., 2002. Cañadón Asfalto, una cuenca de tipo “Pull apart” en el área de Cerro Cóndor. Provincia del Chubut. 15 Congreso Geológico Argentino, Calafate, 238–243.

Silvestro, J., Zubiri, M. 2008. Convergencia oblicua: modelo estructural alternativo para la dorsal Neuquina (39ºs), Neuquén. Revista de la Asociación Geológica Argentina 63, 49-64.

Sparks, R.S.J., 1976. Grain size variations in ignimbrites and implications for the transport of pyroclastic flows. Sedimentology, 23,147–188.

Spinks, K. D.; Acocella, V.; Cole, J. W.; Bassett, K. N., 2005. Structural control of volcanism and caldera development in the transtensional Taupo Volcanic Zone, New Zealand. Journal of Volcanology and Geothermal Research 144, 7-22.

Suárez, M., Márquez, M. 2007. Cuenca de retroarco toarciana en Patagonia central (Chubut), Argentina: cierre, migración del arco y ambiente tectónico durante el Jurásico Medio. Revista Geológica de Chile 34, 1, 63-79.

Stipanicic, P. N., Rodrigo, F., Baulíes, O. and Martínez, C., 1968. Las formaciones presenonianas en el denominado Macizo Nordpatagónico y regiones adyacentes. Revista de la Asociación Geológica Argentina, 23, 2, 67-98.

Streckeisen, A. L., 1976. Classification of the common igneous rocks by means of their chemical composition: a provisional attempt. Neues Jahrbuch fur Mineralogie, Monatshefte, H. l, 1-15.

Sun, S. S., 1982. Chemical composition and origin of the earth´s primitve mantle. Geochemical and Cosmochemical Acta, 46, 179-192.

Sun, S.S., McDonough, W.F., 1989. Chemical and isotopic systematics of oceanic basalts: implication for mantle composition and processes. In: Saunders, A.D., Norry, M.J. (Eds.), Magmatism in the Ocean Basins. Geological Society Special Publication, 42, pp. 313-345.

Thompson, R. N., 1982, Magmatism of the British Tertiary volcanic province: Scottish Journal of Geology, 18, 49-107.

Veiga, R., Lara, M. E., Bruveris, P., 1999. Distribución de hidrocarburos sobre el margen externo en una cuenca de tras-arco. Ejemplos en la cuenca Neuquina, Argentina. Boletín de Informaciones Petroleras 60, 142-164.

Vergani, G., Tankard, A., Belotti, H., Welsink, H. 1995. Tectonic evolution and paleogeography of the Neuquén Basin, Argentina. In: Tankard, A., Suárez, R. and Welsink, H. (Eds.) Petroleum Basins of South America, American Association of Petroleum Geologists, Memoir 62, 383-402.

Uliana, M. A., Biddle, K. T., Cerdán, J., 1989. Mesozoic extension and the formation of Argentina sedimentary basins. In: Tankard, A and Balkwill, H.R. (Eds.) Extensional tectonics and stratigraphy of the North Atlantic margins: AAPG Memoir 46, 599-616.

Walker, G.P.L., 1999. Volcanic rift zones and their intrusion swarms. Journal of Volcanology and Geothermal Research. 94, 21–34.

Winchester, J. A., Floyd, P. A., 1977.Geochemical discrimination of different magma series and their differentiation products using immobile elements. Chemical Geology, 20, 325–343.

Figure captions

Figure 1. Geological sketch of northern Patagonia showing the distribution of pre-Tertiary units outcrops, including Pampean-Famatinian rocks, Gondwana intrusives, Lower and Upper Jurassic volcanites, as well as the Upper Triassic Los Menucos depocenter. The trace of the Huincul fault zone (according to Orchuela and Ploszkiewicz, 1984; Kostadinoff et al., 2005; Gregori et al., 2008) considered as the boundary of the North Patagonian Massif is shown. Location of Figure 2 is also displayed.

Figure 2: Geological map of Cerro Carro Quebrado and Cerro Catri Cura area. The distribution of the Garamilla Formation lithofacies is shown, as well as, profiles, faults, quebradas, cerros and populated places.

Figure 3. A) Typical outcrop of lithofacies I showing a subparallel flow banding. B) Porphyritic texture composed by subhedral crystals of plagioclase and K-feldspar, immersed in a fluidal glassy groundmass. C) Poorly sorted deposit lithofacies II and III, showing a matrix supported breccia and lapilli-tuff of dacitic composition. A 20 cm diameter block of granite appears in the upper portion of lithofacies II.D) Thin section of lithofacies III showing subhedral to anhedral K-feldspar and plagioclase free crystals in a vitrophyric groundmass with abundant ash size lithic fragments. E) Unconformable contact between lithofacies III and lithofacies VI.

Figure 4. A) Lava-like ignimbrites profile (lithofacies IV). Thin basal, fine grained deposits can be recognized underlying the thick massive deposits. B) Thin

section of lithofacies IV showing neoformation of subhedral to euhedral crystals of quartz indicating static recrystallization. C) Lithofacies V showing diffuse to massive stratification, 500 m southward the Cerro Pafaniyeu. D) Thin section of lithofacies V showing crystal-rich and well preserved eutaxitic textures.

Figure 5. Lava dome (lithofacies VI, VII and VIII) distribution at the margins of the Cerro Carro Quebrado and Cerro Catri Cura area showing a half-moon pattern.

Figure 6. A) Representative outcrop of flow banded rhyolite (lithofacies VI) displaying spherulites-rich and poor bands. B) Fine grained 250 μm diameter spherulitic aggregates immersed in a felsitic groundmass (lithofacies VI). C) Relationships of lithofacies VI, VII and VIII in a rhyolitic lava dome. Massive rhyolite facies form the central part passing laterally to the flow banded and autoclastic facies which represent the external border of the body. D) Static recrystallization of quartz crystals in the groundmass. E) Typical outcrop of autoclastic facies (lithofacies VIII) formed by subangular to angular, 6 to 20 cm long fragments of rhyolitic composition of the massive and flow banded facies.

Figure 7. A) U–Pb zircon provenance age patterns for sample DN4 (upper part of lithofacies III) east of Cerro Carro Quebrado. The curve in the diagram is relative probability trends based on the preferred age derived from individual measurements, which are also shown. $^{206}Pb/^{238}U$ ages for values less than 1000 Ma were used. Diagram of sample Q16 from Quiñenao are is shown for comparison. B) $^{206}Pb/^{238}U$ vs. $^{207}Pb/^{235}U$ concordia diagram for sample DN4. C)

Probabilistic plot of $^{206}Pb/^{238}U$ ages displaying the “best age” for Garamilla Formation.

Figure 8. A) A high potassium calc-alkaline trend is displayed by the samples in the Peccerillo and Taylor, (1976) diagram. B) Dacitic and rhyolitic compositions are dominant in the K_2O and Na_2O versus silica diagram (Le Bas et al., 1986). C) A similar results is showed by the Cox et al., (1979) diagram. D) Plotted in an AFM diagram (Irvine and Baragar, 1971) samples display a calc-alkaline tendency. E) Streckeisen (1976) diagram showing that most rocks range from dacites to alkaline rhyolites, with 4 samples of acidic dykes being alkaline rhyolites.

Figure 9. A) SiO_2 versus Zr/TiO_2 diagram of Winchester and Floyd (1977) displaying rhyodacitic-dacitic to rhyolitic compositions. B) Zr/Ti versus Nb/Y diagram of Winchester and Floyd (1977) showing a more varied chemical composition including trachyandesitic members. C) Chondrite-normalized expanded diagrams (Thompson, 1982) showing enrichment in LILE and depletion of Sr, P and Ti. Negative anomaly of Nb and Ta relative to Th and La, are considered as subduction zone signature. D) Chondrite-normalized diagrams (Sun and McDonough, 1989) displaying moderate negative Eu anomalies associated with fractionation of plagioclase and a cogenetic character of the rocks. E) The Th/Yb vs Ta/Yb diagram (Pearce, 1983) indicates a shoshonitic signature for the analyzed samples, with a within- plate evolution. F) Nb versus Y diagram (Pearce et al., 1984) where samples plot in the field of magmatic arc-related rocks.

Figure 10. Geological sketch of the 40°10' S- 40°2 3' S and 69°42' W- 70°02' W area of the western sector of the North Patagonian Massif showing the south, central and northern complexes of acidic dykes. Dip-azimuth pole to plane data frequency were plotted in the lower hemisphere stereographic circle combined with rose diagram, indicating azimuth of dykes. Each diagram (I to VI) is explained in the text.

Figure 11. Composite profile for the Garamilla Formation in the Cerro Carro Quebrado and Cerro Catri Cura area, western North Patagonian Massif. Eight lithofacies were recognized from stage 1, pre-Pliesbachian andesites related to dilatational zones to stage 4 integrated by lava flows, lava-domes and dykes of rhyolitic composition.

Figure 12. Schematic cartoon displaying the four stages in the evolution of the magmatic system. Stage I was recognized in limited areas and represents a pre-collapse, not subsidence event. Stage II represents a more extensive event that includes opening and development of a volcanic caldera with depositation of pyroclastic sequences. Stage III is formed by lava-like ignimbrites, and massive lapilli- tuffs that represent a major volcanic collapse with caldera infilling. The last stage includes post-collapse dome and dykes development.

Figure 13. A) Swarms of dykes showing seudo-parallel and en-echelon system designs at 40°10' S- 40°23' S and 69°42' W - 70°02' W in the western North Patagonian Massif. B) Agostini et al., (2009) and Corti, (2012) model for the beginning of the extension for a highly oblique rift. In-echelon, border faults

and rift-parallel faults are not developed. C) Agostini et al., (2009) and Corti, (2012) model for a more developed extensional system. Rift-parallel faults and in-echelon, border faults are present. In our study area, dyke swarms are interpreted as in-echelon, border faults and internal curved faults, roughly orthogonal to the extension.

Table caption request

Table 1: U-Pb geochronological analyses of DN4 sample.

Table 2: Chemical composition of Cerro Carro Quebrado and Cerro Catri Cura area analyzed samples.

Table 1. U-Pb geochronological analyses.

Analysis	U (ppm)	$^{206}Pb/^{204}Pb$	U/Th	$^{206}Pb^{*}/^{207}Pb^{*}$	± (%)	$^{207}Pb^{*}/^{235}U^{*}$	± (%)	$^{206}Pb^{*}/^{238}U$	± (%)	error corr.	$^{206}Pb^{*}/^{238}U^{*}$	± (Ma)	$^{207}Pb^{*}/^{235}U$	± (Ma)	$^{206}Pb^{*}/^{207}Pb^{*}$	± (Ma)	Best age (Ma)	± (Ma)
DN4 1C	208	28953	2.2	20.9108	9.5	0.1929	10.1	0.0293	3.5	0.35	185.9	6.5	179.1	16.6	90.5	224.5	185.9	6.5
DN4 10R	167	29196	1.9	19.9632	12.7	0.2022	12.9	0.0293	2.3	0.18	186.0	4.2	186.9	22.1	199.3	296.5	186.0	4.2
DN4 20R	197	45203	2.0	19.7781	9.6	0.2045	9.8	0.0293	2.0	0.21	186.4	3.7	188.9	16.9	220.9	222.3	186.4	3.7
DN4 10C	180	23150	1.6	22.2345	5.9	0.1825	6.5	0.0294	2.7	0.41	187.0	4.9	170.2	10.1	-57.0	143.5	187.0	4.9
DN4 6R	315	33307	2.5	21.0175	6.5	0.1934	6.9	0.0295	2.4	0.34	187.3	4.3	179.5	11.4	78.4	155.0	187.3	4.3
DN4 8R	436	60565	1.4	19.5187	4.8	0.2087	4.9	0.0295	1.2	0.23	187.7	2.1	192.5	8.7	251.3	110.7	187.7	2.1
DN4 14C	216	36888	1.6	20.0169	13.1	0.2041	13.9	0.0296	4.6	0.33	188.2	8.5	188.6	23.9	193.0	305.3	188.2	8.5
DN4 19C	167	40477	1.4	21.3753	16.5	0.1915	16.6	0.0297	2.0	0.12	188.6	3.7	177.9	27.1	38.1	396.7	188.6	3.7
DN4 2C	151	23023	1.3	20.1146	12.0	0.2038	12.3	0.0297	2.7	0.22	188.8	5.1	188.3	21.2	181.7	281.1	188.8	5.1
DN4 14R	157	36428	1.9	20.1933	9.3	0.2031	9.6	0.0298	2.4	0.25	189.0	4.5	187.8	16.5	172.6	217.8	189.0	4.5
DN4 12C	175	25602	1.6	20.7658	17.8	0.1985	18.1	0.0299	3.2	0.18	189.9	5.9	183.9	30.4	107.0	422.8	189.9	5.9
DN4 7C	206	33846	1.2	21.0558	12.2	0.1959	12.6	0.0299	3.4	0.27	190.0	6.4	181.6	21.0	74.1	290.5	190.0	6.4
DN4 3C	608	156288	16.5	20.6844	5.7	0.1996	5.9	0.0299	1.4	0.24	190.2	2.7	184.8	10.0	116.2	135.1	190.2	2.7
DN4 6C	274	39085	2.8	19.5812	10.8	0.2109	11.2	0.0300	3.3	0.29	190.3	6.1	194.3	19.9	244.0	248.4	190.3	6.1
DN4 19R	131	23380	2.2	19.3998	9.7	0.2129	11.2	0.0300	5.6	0.50	190.3	10.5	196.0	20.0	265.4	223.0	190.3	10.5
DN4 2R	334	46136	1.2	20.0006	7.8	0.2066	8.0	0.0300	1.7	0.21	190.4	3.2	190.7	13.9	194.9	182.1	190.4	3.2
DN4 12R	269	30143	1.3	20.6653	9.4	0.2003	9.5	0.0300	1.7	0.18	190.7	3.2	185.4	16.1	118.4	221.2	190.7	3.2
DN4 3R	651	158791	23.2	19.9454	3.7	0.2075	3.9	0.0300	1.1	0.29	190.7	2.1	191.5	6.8	201.3	86.5	190.7	2.1
DN4 1R	108	11109	2.4	18.4781	11.2	0.2249	11.7	0.0301	3.1	0.26	191.5	5.8	206.0	21.7	375.9	253.8	191.5	5.8
DN4 7R	535	95073	1.1	20.4511	4.5	0.2033	4.8	0.0302	1.6	0.34	191.5	3.0	187.9	8.3	142.9	106.6	191.5	3.0
DN4 17R	799	160242	0.7	20.3748	2.2	0.2045	2.9	0.0302	1.9	0.65	191.9	3.5	188.9	5.0	151.7	51.7	191.9	3.5
DN4 11R	2979	127785	2.3	19.9744	0.8	0.2149	1.7	0.0311	1.5	0.90	197.7	3.0	197.7	3.1	198.0	17.6	197.7	3.0
DN4 11C	267	13192	2.0	20.1838	5.6	0.2134	6.1	0.0312	2.4	0.39	198.3	4.6	196.4	10.9	173.7	131.1	198.3	4.6
DN4 20C	117	10901	1.9	18.6920	14.4	0.2272	14.9	0.0308	3.8	0.25	195.6	7.3	207.9	28.0	350.0	327.4	195.6	7.3
DN4 9R	123	16214	0.9	18.8730	18.8	0.2156	19.1	0.0295	3.2	0.17	187.5	6.0	198.3	34.4	328.2	430.2	187.5	6.0
DN4 16C	91	15401	1.0	20.6643	28.3	0.1947	28.6	0.0292	4.4	0.15	185.4	8.0	180.6	47.4	118.5	678.3	185.4	8.0
DN4 16R	77	10668	1.0	20.1781	39.6	0.2044	39.9	0.0299	5.0	0.13	190.0	9.4	188.9	68.8	174.3	957.1	190.0	9.4
DN4 5R	92	10111	1.2	22.6671	22.5	0.1783	22.7	0.0293	3.1	0.13	186.3	5.6	166.6	34.9	-104.1	559.4	186.3	5.6
DN4 5C	55	13384	2.4	24.7297	26.1	0.1659	27.1	0.0298	7.1	0.26	189.1	13.2	155.9	39.1	-322.9	679.8	189.1	13.2
DN4 15C	80	17482	1.0	18.1407	22.6	0.2291	23.3	0.0301	5.6	0.24	191.5	10.5	209.5	44.1	417.3	511.0	191.5	10.5
DN4 18R	36	3429	2.2	35.1949	103.0	0.1182	103.2	0.0302	6.5	0.06	191.6	12.3	113.4	111.2	NA	NA	191.6	12.3
DN4 18C	37	4545	2.0	17.6521	95.3	0.2232	95.6	0.0286	7.0	0.07	181.6	12.6	204.5	178.9	477.9	632.1	181.6	12.6
DN4 9C	72	3037	1.0	18.6270	22.6	0.2248	23.5	0.0304	6.3	0.27	192.8	12.1	205.9	43.8	357.9	516.5	192.8	12.1

Table 2. Geochemical analyses

Sample	C18	C20	C34	C1	M21	M11	M41	M46	M25	M38C	J26	M24
SiO2	74.43	66.11	71.47	72.32	67.58	75.72	75.98	74.86	77.31	71.83	68.89	78.53
Al2O3	13.33	15.02	13.98	14.29	14.1	12.05	12.21	12.59	12.11	12.97	14.3	11.23
Fe2O3(T)	2.14	4.13	2.43	2.62	3.29	1.75	1.54	1.41	1.24	2.52	2.98	1.75
MnO	0.053	0.083	0.072	0.05	0.053	0.022	0.017	0.011	0.012	0.046	0.061	0.018
MgO	0.49	1.17	0.43	0.38	0.92	0.1	0.09	0.11	0.08	0.43	0.72	0.1
CaO	1.08	3.98	1.58	1.9	2.74	0.2	0.19	0.21	0.11	1.13	2.27	0.14
Na2O	3.38	3.27	2.92	3.49	3.32	3.13	3.11	4.26	2.16	2.82	3.68	3.82
K2O	4.13	2.84	4.13	3.76	3.15	4.66	4.41	3.87	4.32	4.95	3.41	3.73
TiO2	0.249	0.503	0.284	0.293	0.323	0.074	0.077	0.052	0.043	0.267	0.381	0.061
P2O5	0.07	0.15	0.07	0.07	0.07	0.02	0.01	0.01	0.02	0.07	0.11	0.01
LOI	1.22	1.58	2.45	0.78	3.79	0.94	1.2	1.04	1.51	1.82	3	0.74
Total	100.6	98.82	99.83	99.96	99.34	98.66	98.84	98.42	98.91	98.85	99.8	100.1
Sc	4	12	7	8	7	3	3	3	3	4	5	3
V	23	47	23	20	54	9	5	10	5	24	40	5
Ba	1156	699	1176	967	434	1030	1017	438	1039	992	864	1415
Sr	159	324	206	222	149	93	94	60	70	173	220	114
Y	18	23	26	24	14	23	16	14	21	21	22	19
Zr	132	257	178	209	113	83	83	58	54	156	186	75
Co	3	7	5	5	5	1	3	1	1	2	3	1
Ga	14	19	16	17	19	14	15	13	15	15	18	12
Ge	1	2	2	2	1	1	1	1	1	1	1	1
Rb	155	103	140	154	167	171	167	136	203	219	147	129
Nb	8	9	8	10	10	10	8	12	9	10	9	8
Sn	3	3	3	4	7	4	4	6	6	5	3	3
Cs	5.3	3.1	6.4	4.7	9.2	4.2	3	2.6	6.2	4.5	4.7	2.3
La	29.5	37.8	37.6	36.7	19.7	26.7	13.8	8.7	20.1	29.7	31.2	31.6
Ce	57.2	75.8	72.6	74	38.5	51.8	25.7	16.2	34.1	58.4	61.1	55.5
Pr	6.22	8.67	8.18	8.43	4.4	5.47	3.2	2.44	4.87	6.69	7.04	6.7
Nd	23.1	34.1	31.4	32.9	16.4	18.9	10.9	8	17	23.5	24.3	22.7
Sm	4.4	6.5	6.2	6.5	3.9	3.9	2.3	2	3.8	4.7	4.8	4.3
Eu	0.71	1.79	1.26	1.36	0.67	0.58	0.38	0.15	0.54	0.78	1.1	0.59
Gd	3.3	5.2	4.8	4.9	3.3	3.8	2.3	1.5	3.5	4	4	3.4
Tb	0.5	0.8	0.8	0.8	0.5	0.6	0.4	0.3	0.6	0.6	0.6	0.6
Dy	2.9	4.5	4.4	4.3	2.6	3.7	2.5	2.2	3.5	3.8	3.7	3.3
Ho	0.6	0.9	0.9	0.9	0.5	0.7	0.5	0.5	0.7	0.7	0.7	0.6
Er	1.8	2.6	2.7	2.6	1.4	2.1	1.6	1.5	2.1	2.2	2.2	1.9
Tm	0.29	0.38	0.41	0.39	0.2	0.31	0.25	0.26	0.32	0.34	0.33	0.31
Yb	2.1	2.5	2.8	2.7	1.4	2	1.7	2	2.2	2.4	2.3	2.1
Lu	0.34	0.41	0.47	0.44	0.22	0.31	0.28	0.38	0.36	0.41	0.4	0.35
Hf	3.6	6.1	4.6	5.4	3.3	2.6	2.6	2.5	2.2	4.3	4.6	2.5
Ta	0.8	0.7	0.8	0.8	1.3	1.1	1.1	1.3	1.1	1.1	0.9	0.8
Pb	16	16	24	22	54	39	9	25	17	20	26	36
Th	14	10.2	13.4	13	10.8	12.2	11.8	12.5	10.3	13.6	11.2	14.7
U	2.6	2	3.1	2.9	4.2	3.6	2.6	4.9	4.2	2.9	3	3.2

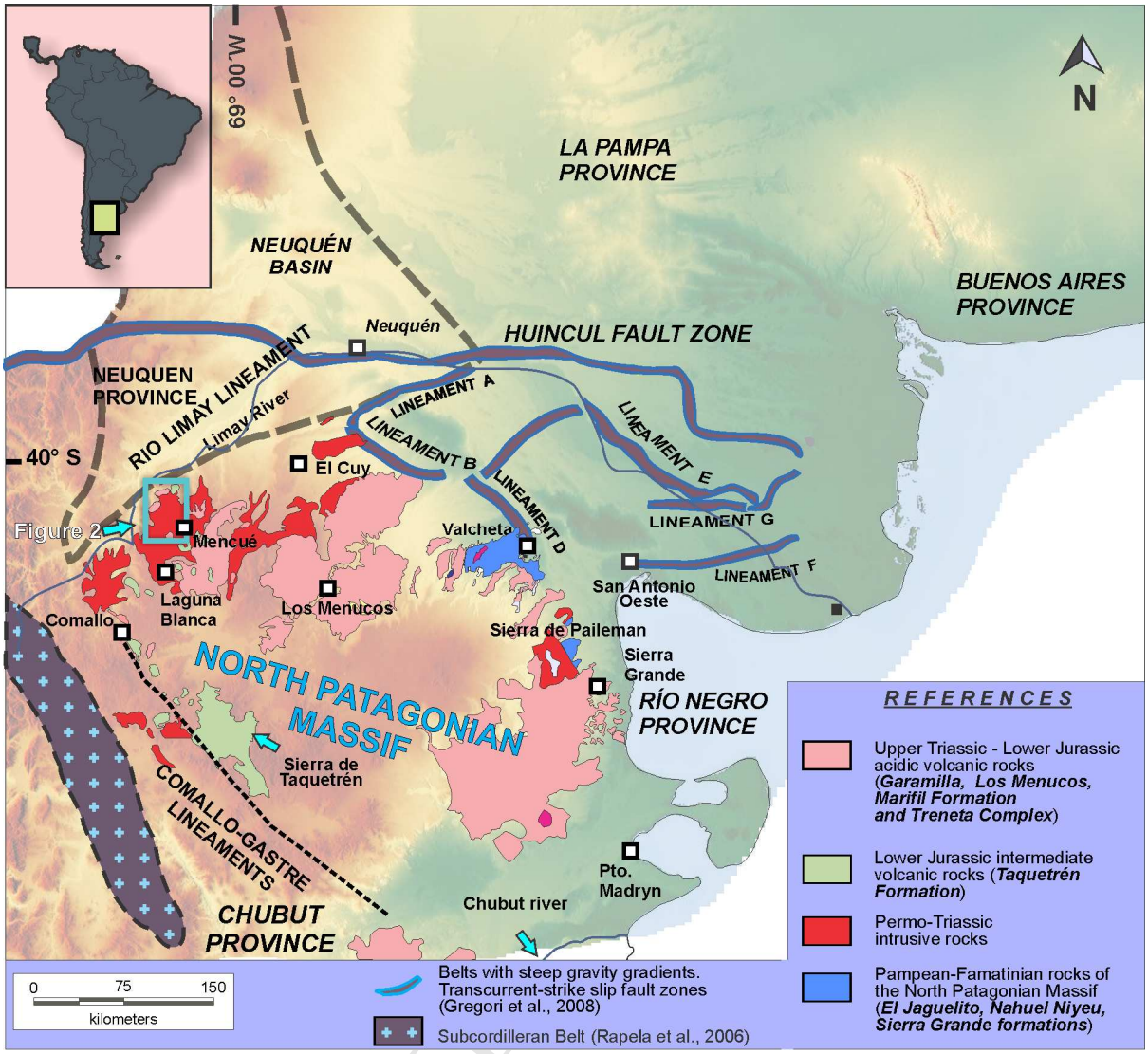
69° W
N
LA PAMPA PROVINCE
NEUQUÉN BASIN
BUENOS AIRES PROVINCE
Neuquén
HUINCUL FAULT ZONE
NEUQUEN PROVINCE
RIO LIMAY LINEAMENT
Limay River
LINEAMENT A
LINEAMENT B
LINEAMENT D
LINEAMENT E
LINEAMENT G
LINEAMENT F
40° S
El Cuy
Figure 2
Mencué
Laguna Blanca
Comallo
Los Menucos
Valcheta
San Antonio Oeste
Sierra de Paileman
Sierra Grande
RÍO NEGRO PROVINCE
NORTH PATAGONIAN MASSIF
Sierra de Taquetrén
COMALLO-GASTRE LINEAMENTS
CHUBUT PROVINCE
Chubut river
Pto. Madryn
0 75 150
kilometers
Belts with steep gravity gradients. Transcurrent-strike slip fault zones (Gregori et al., 2008)
Subcordilleran Belt (Rapela et al., 2006)
REFERENCES
Upper Triassic - Lower Jurassic acidic volcanic rocks (Garamilla, Los Menucos, Marifil Formation and Treneta Complex)
Lower Jurassic intermediate volcanic rocks (Taquetrén Formation)
Permo-Triassic intrusive rocks
Pampean-Famatinian rocks of the North Patagonian Massif (El Jaguelito, Nahuel Niyeu, Sierra Grande formations)

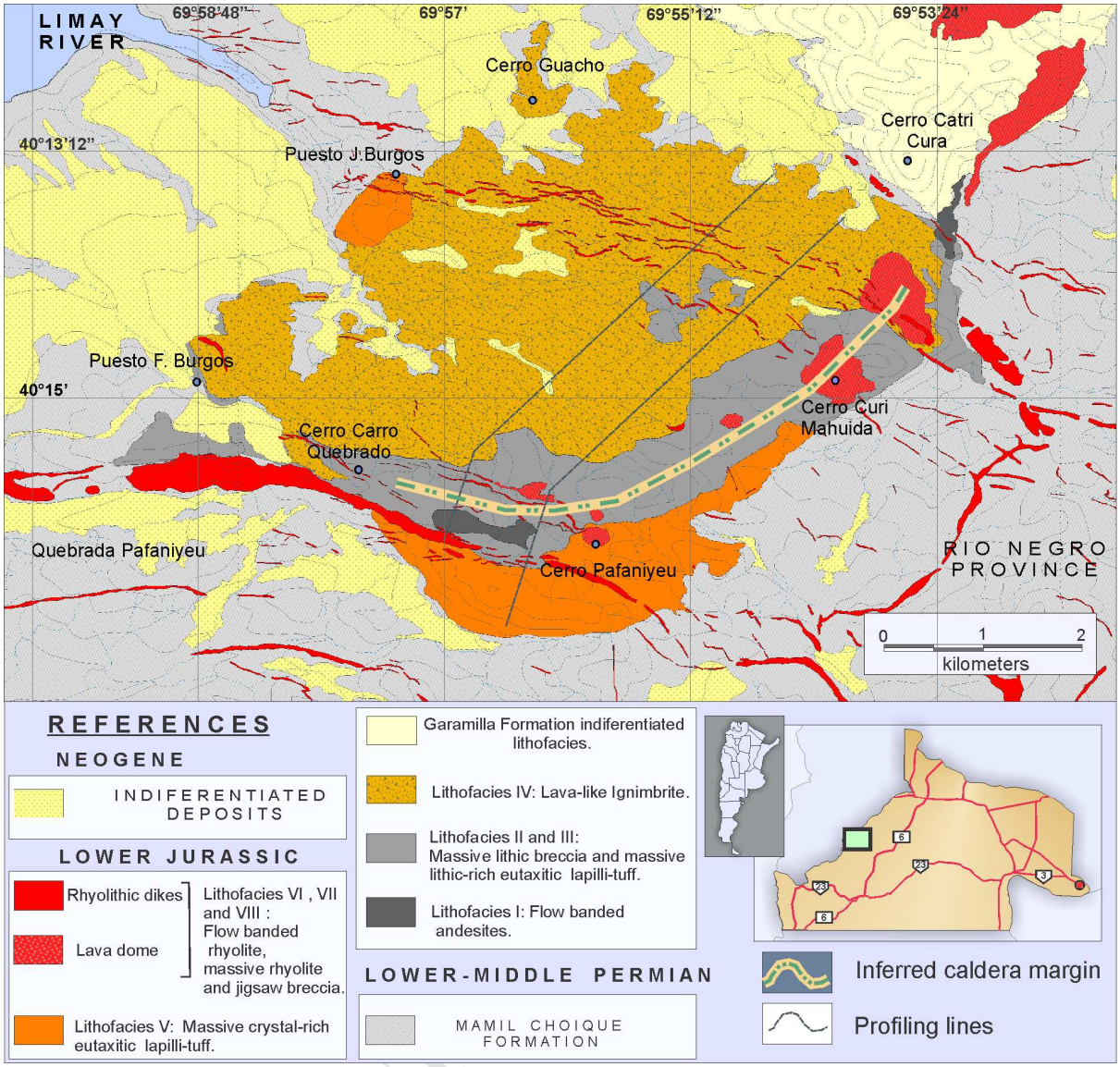
LIMAY RIVER
69°58'48"
69°57'
69°55'12"
69°53'24"
40°13'12"
40°15'
Cerro Guacho
Puesto J. Burgos
Cerro Catri Cura
Puesto F. Burgos
Cerro Curi Mahuida
Cerro Carro Quebrado
Quebrada Pafaniyeu
Cerro Pafaniyeu
RIO NEGRO PROVINCE
0
1
2
kilometers
REFERENCES
NEOGENE
INDIFERENTIATED DEPOSITS
LOWER JURASSIC
Rhyolithic dikes
Lava dome
Lithofacies VI , VII and VIII : Flow banded rhyolite, massive rhyolite and jigsaw breccia.
Lithofacies V: Massive crystal-rich eutaxitic lapilli-tuff.
Garamilla Formation indiferentiated lithofacies.
Lithofacies IV: Lava-like Ignimbrite.
Lithofacies II and III: Massive lithic breccia and massive lithic-rich eutaxitic lapilli-tuff.
Lithofacies I: Flow banded andesites.
LOWER-MIDDLE PERMIAN
MAMIL CHOIQUE FORMATION
Inferred caldera margin
Profiling lines

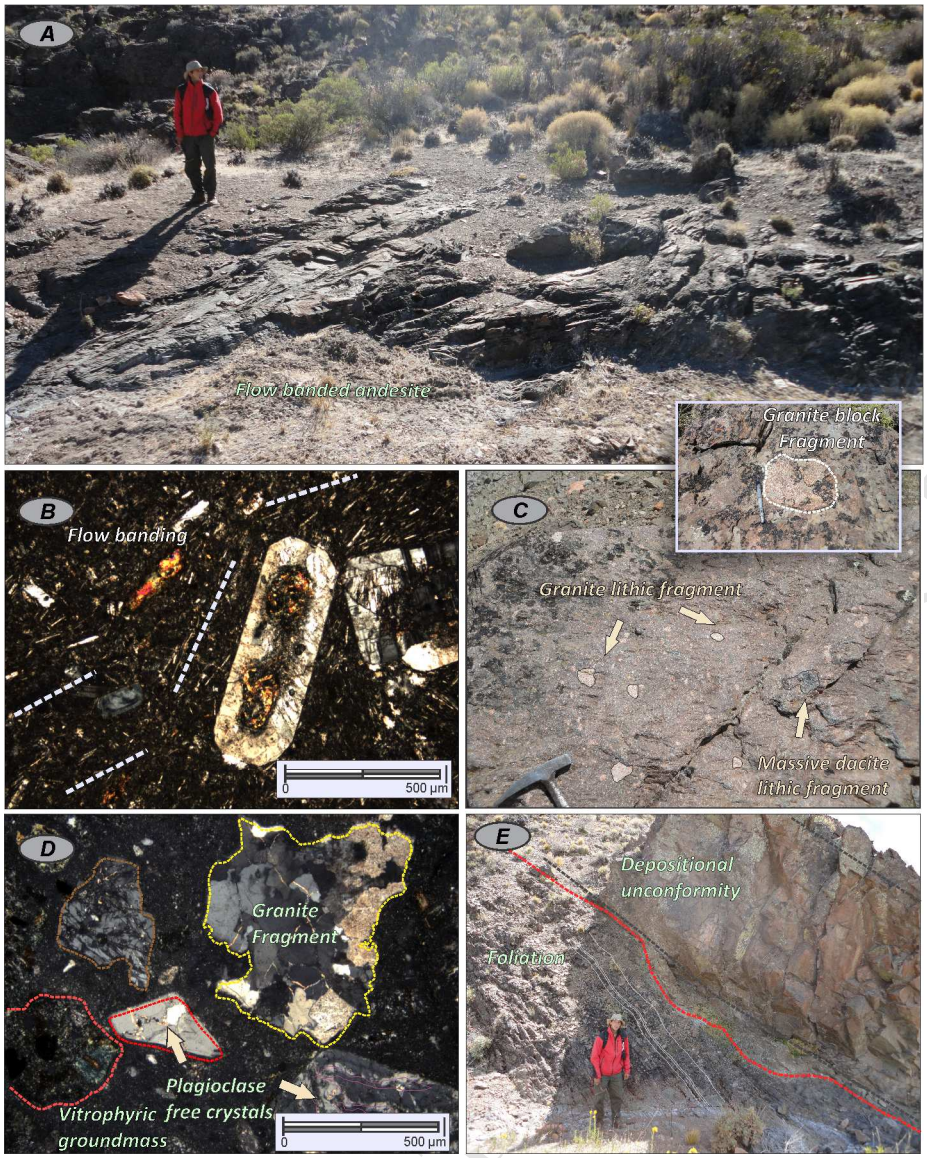

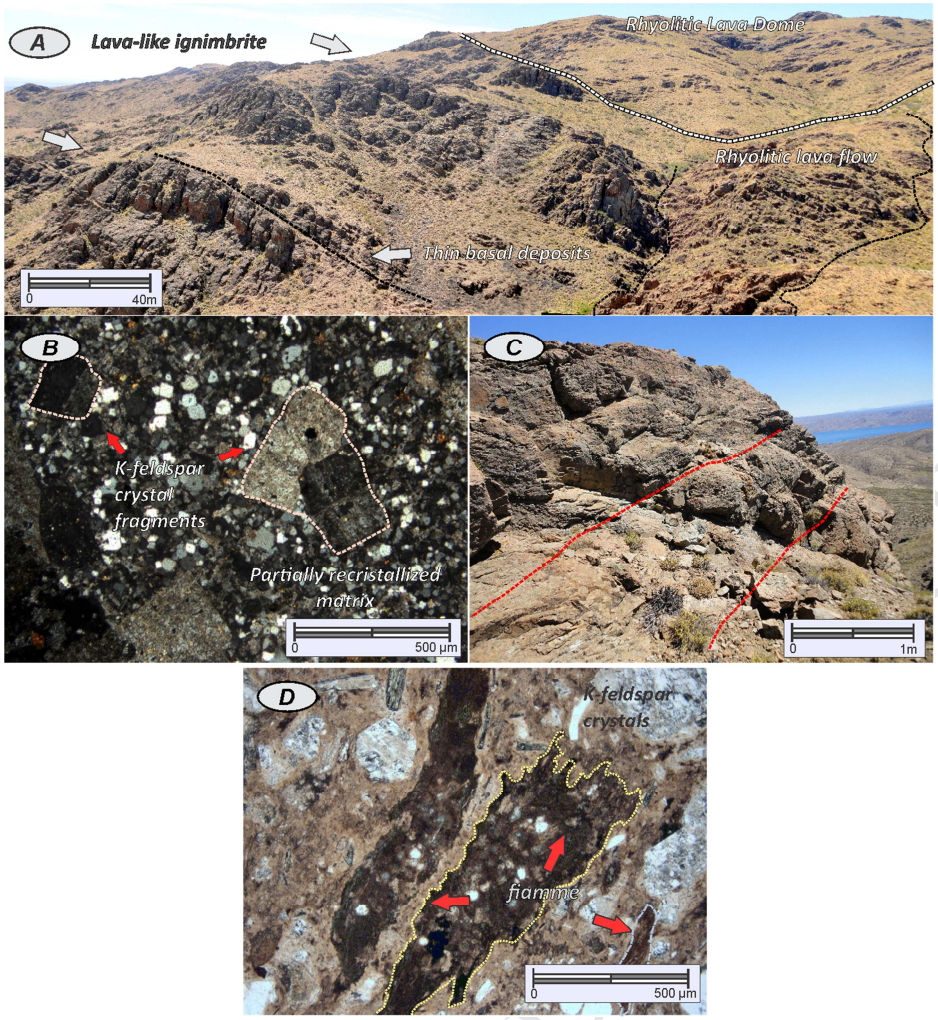

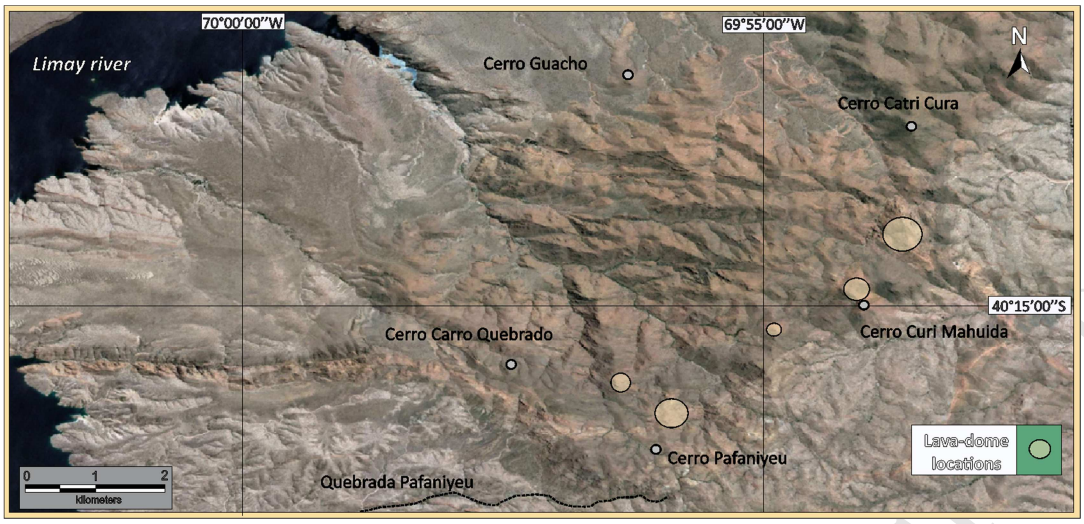

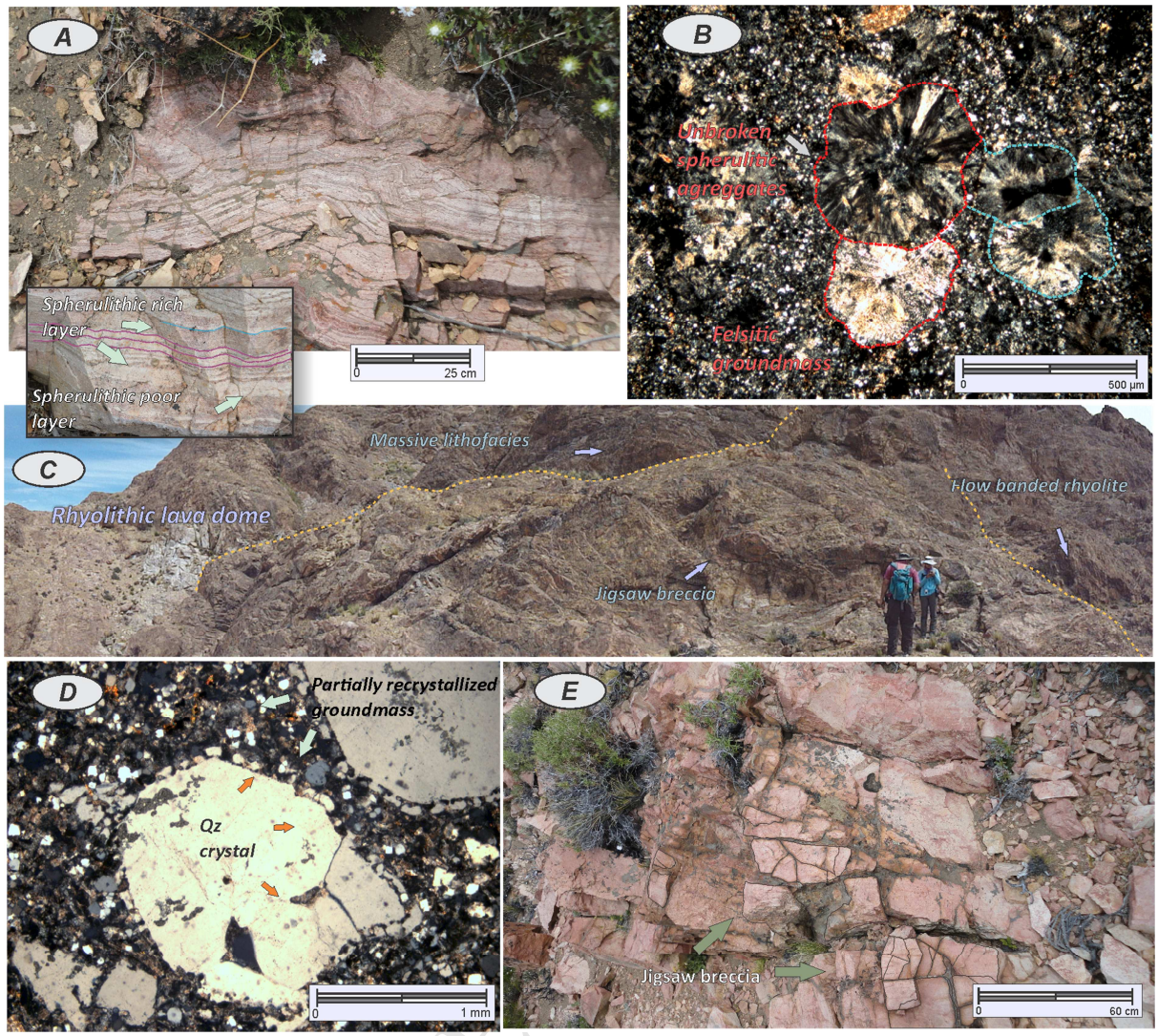
A
Spherulithic rich layer
Spherulithic poor layer
0
25 cm
B
Unbroken spherulitic agreggates
Felsitic groundmass
0
500 µm
C
Massive lithofacies
Rhyolithic lava dome
Flow banded rhyolite
Jigsaw breccia
D
Partially recrystallized groundmass
Qz crystal
0
1 mm
E
Jigsaw breccia
0
60 cm

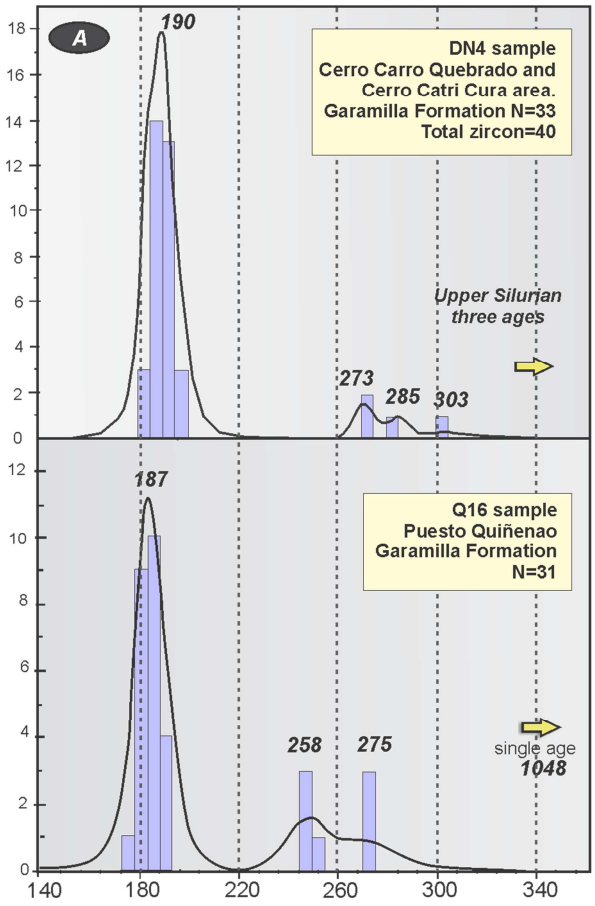

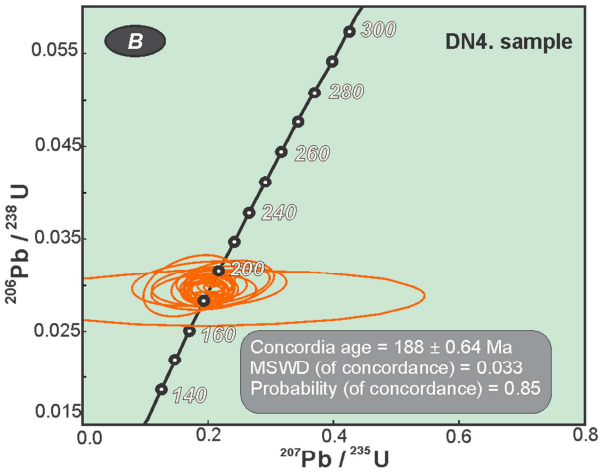

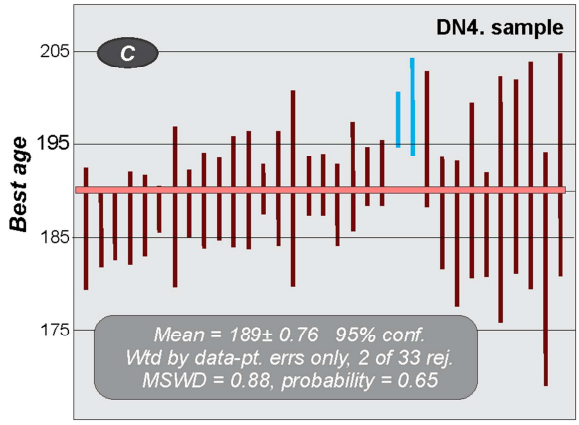

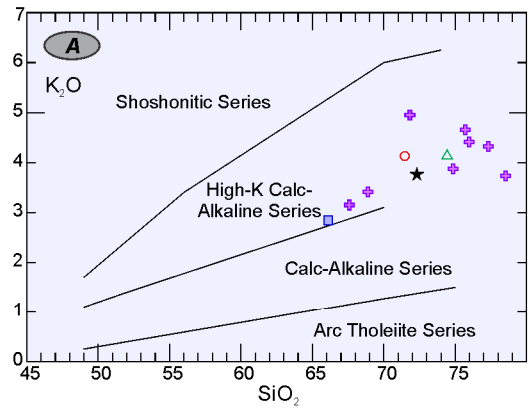

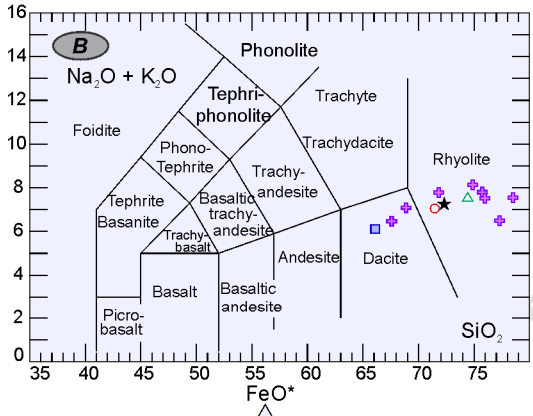

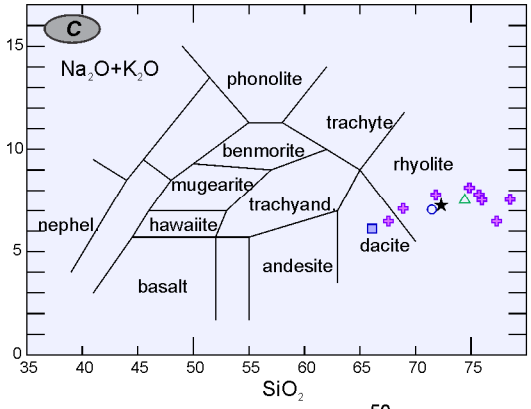

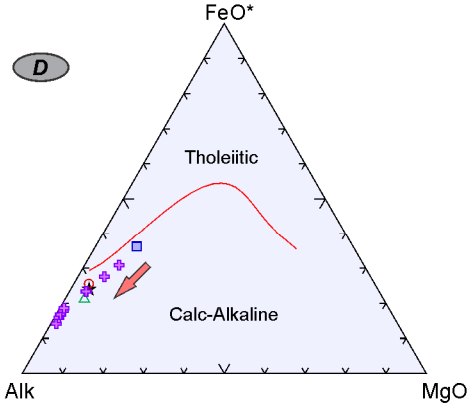

Lithofacies V, VI and VII:
Flow banded rhyolite, massive rhyolite and jigsaw Breccia.

Lithofacies V:
Massive eutaxitic lapilli-Tuff

Lithofacies IV:
Lava like ignimbrite

Lithofacies III:
Massive eutaxitic lapilli-Tuff lithofacies

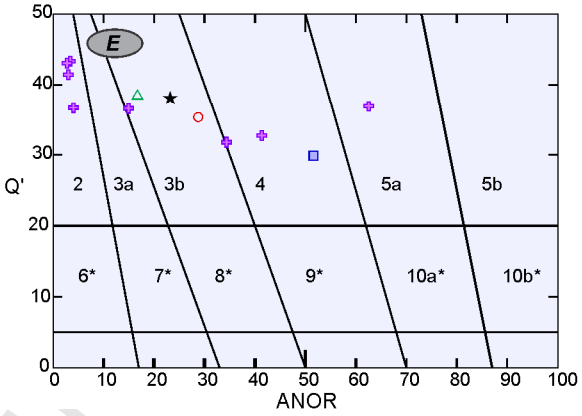

2 alkali rhyolite
3 rhyolite
4 dacite
5 (dacite)
6 trachyte
7 Q trachyte
8 Q latite
9 andesite
10 basalt

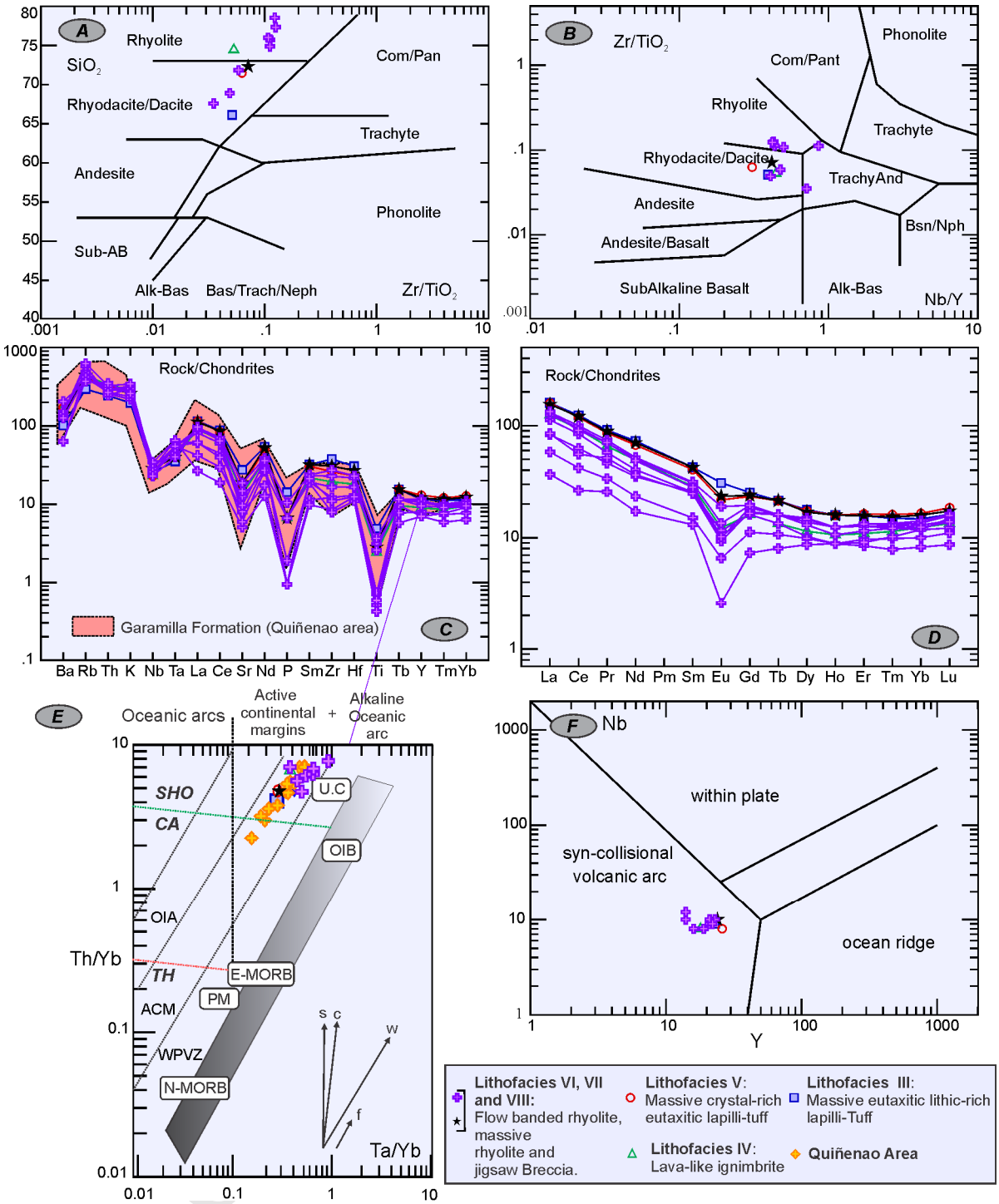
A
Rhyolite
SiO2
Com/Pan
Rhyodacite/Dacite
Trachyte
Andesite
Phonolite
Sub-AB
Alk-Bas
Bas/Trach/Neph
Zr/TiO2
B
Zr/TiO2
Phonolite
Com/Pant
Rhyolite
Trachyte
Rhyodacite/Dacite
TrachyAnd
Andesite
Bsn/Nph
Andesite/Basalt
SubAlkaline Basalt
Alk-Bas
Nb/Y
C
Rock/Chondrites
Garamilla Formation (Quiñenao area)
Ba Rb Th K Nb Ta La Ce Sr Nd P SmZr Hf Ti Tb Y TmYb
D
Rock/Chondrites
La Ce Pr Nd Pm Sm Eu Gd Tb Dy Ho Er Tm Yb Lu
E
Oceanic arcs
Active continental margins
+
Alkaline Oceanic arc
SHO
CA
TH
OIA
ACM
WPVZ
N-MORB
E-MORB
PM
U.C
OIB
Th/Yb
Ta/Yb
s c
w
f
F
Nb
within plate
syn-collisional volcanic arc
ocean ridge
Y
Lithofacies VI, VII and VIII: Flow banded rhyolite, massive rhyolite and jigsaw Breccia.
Lithofacies V: Massive crystal-rich eutaxitic lapilli-tuff
Lithofacies III: Massive eutaxitic lithic-rich lapilli-Tuff
Lithofacies IV: Lava-like ignimbrite
Quiñenao Area

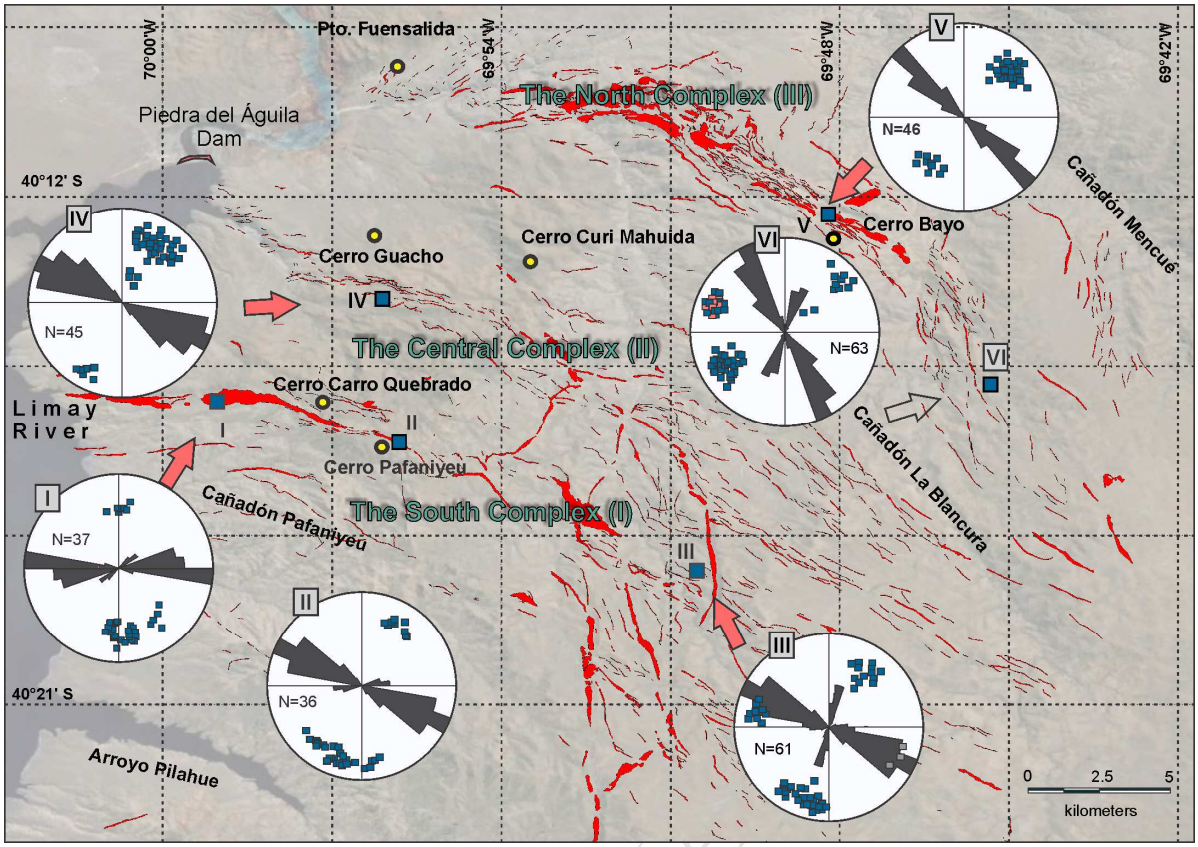

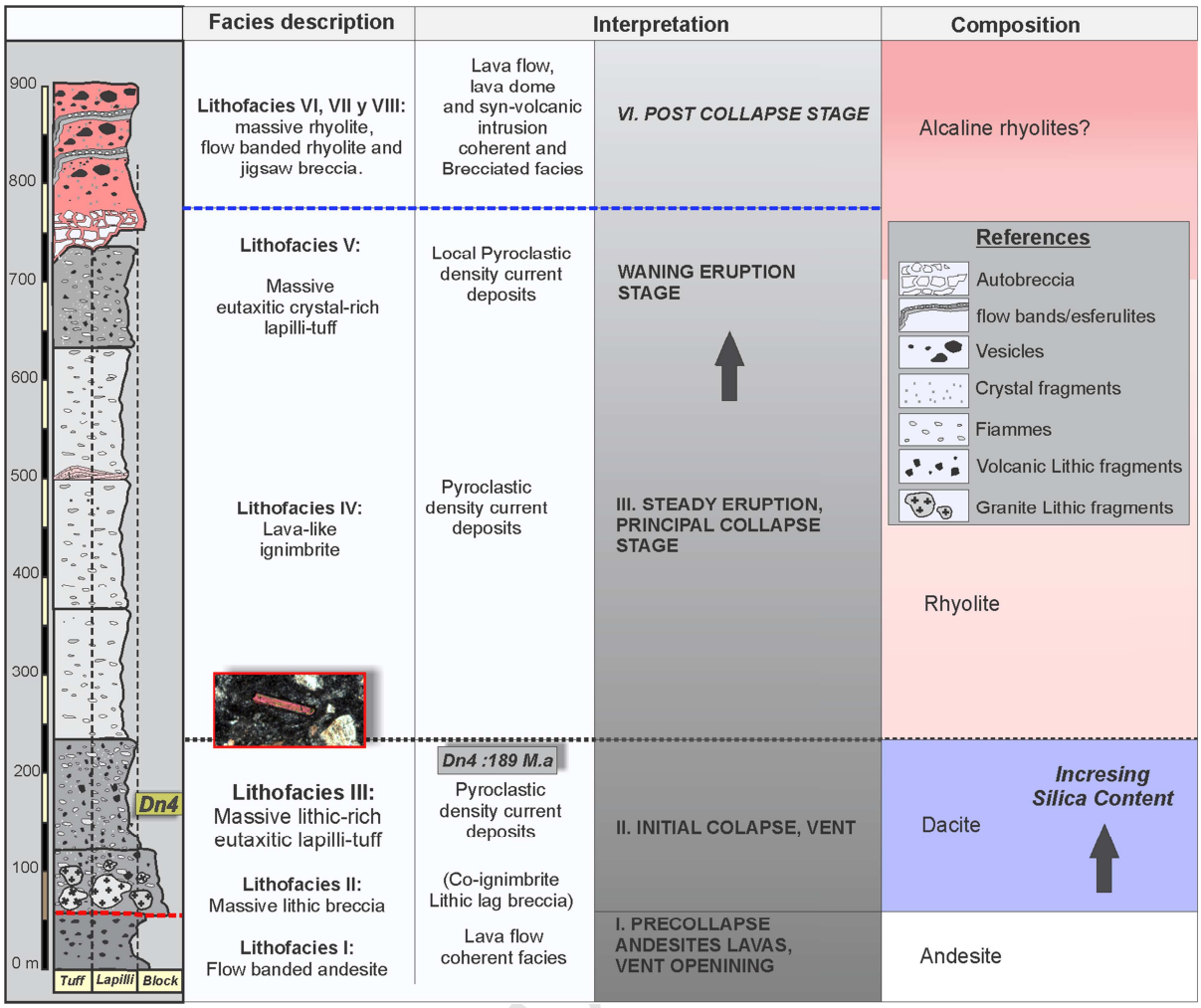

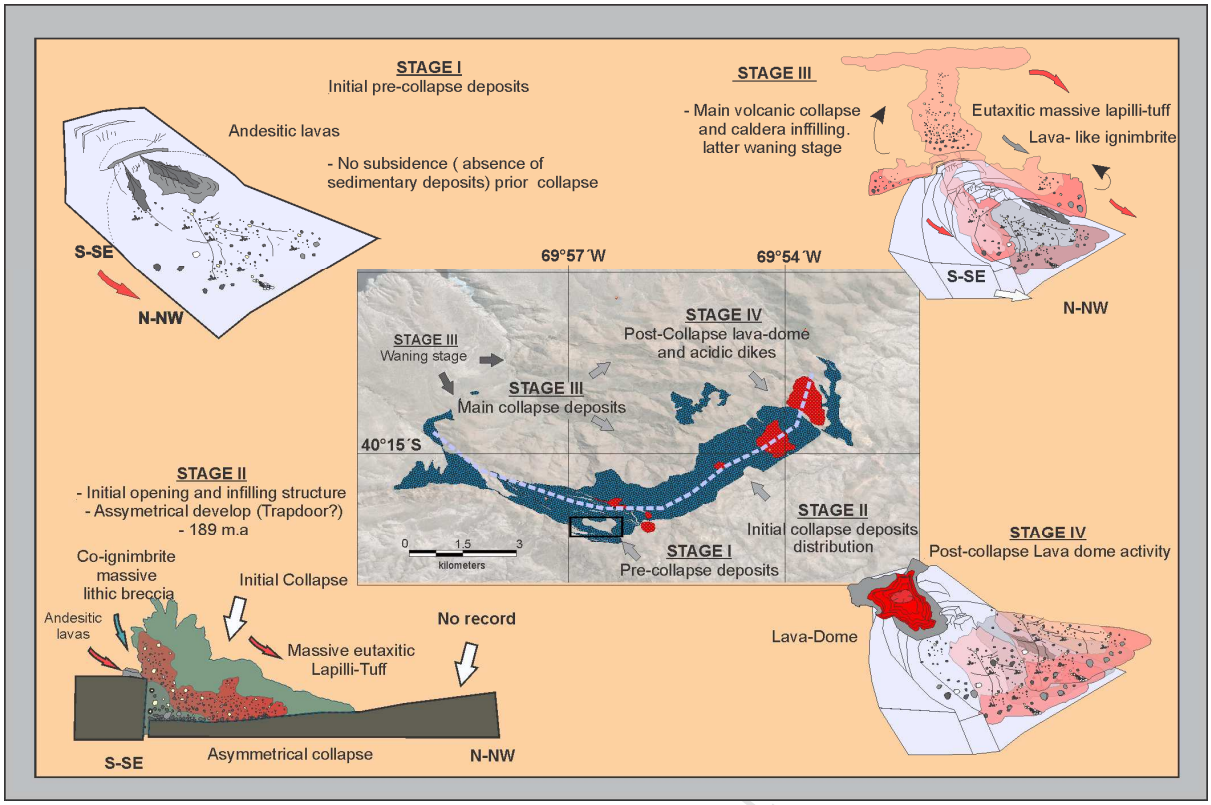

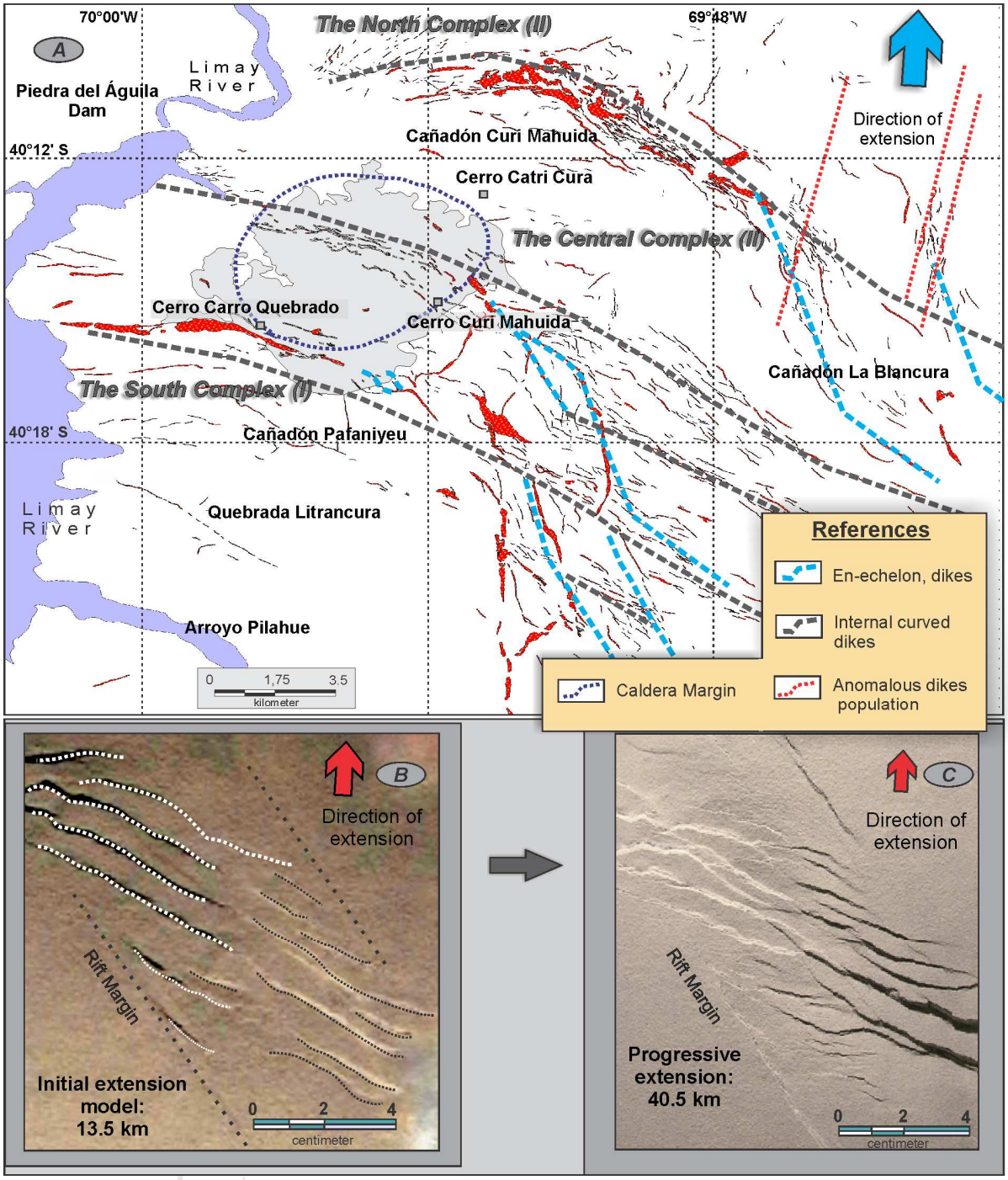
70°00'W
69°48'W
A
Piedra del Águila Dam
Limay River
The North Complex (II)
Cañadón Curi Mahuida
Direction of extension
40°12' S
Cerro Catri Cura
The Central Complex (II)
Cerro Carro Quebrado
Cerro Curi Mahuida
Cañadón La Blancura
The South Complex (I)
40°18' S
Cañadón Pafaniyeu
Limay River
Quebrada Litrancura
Arroyo Pilahue
0 1,75 3.5
kilometer
References
En-echelon, dikes
Internal curved dikes
Caldera Margin
Anomalous dikes population
B
Direction of extension
Rift Margin
Initial extension model: 13.5 km
0 2 4
centimeter
C
Direction of extension
Rift Margin
Progressive extension: 40.5 km
0 2 4
centimeter

Research highlights

- The Garamilla Formation was studied near the Limay river in the western North Patagonian Massif.
- It is composed of four volcanic stages from andesitic to rhyolitic compositions.
- Radiometric dating indicates Pliensbachian age for the initiation of the volcanic system.
- Field evidences support a caldera volcanism in high- obliquity rift systems during Jurassic times.